Title
LONGITUDINAL DISPERSION IN PACKED EXTRACTION COLUMNS

Authors
Jacques, Gabriel L.
Cotter, John E.
Vermeulen, Theodore.

Publication Date
1959-04-01

UCRL 8658

UNIVERSITY OF
CALIFORNIA
Ernest O. Lawrence
Radiation Laboratory

LONGITUDINAL DISPERSION IN PACKED EXTRACTION COLUMNS

DISCLAIMER

UCRL-8658

UNIVERSITY OF CALIFORNIA

Lawrence Radiation Laboratory
Berkeley, California

Contract No. W-7405-eng-48

LONGITUDINAL DISPERSION IN PACKED EXTRACTION COLUMNS

Gabriel L. Jacques, John E. Cotter,
and Theodore Vermeulen

April, 1959

Printed for the U. S. Atomic Energy Commission

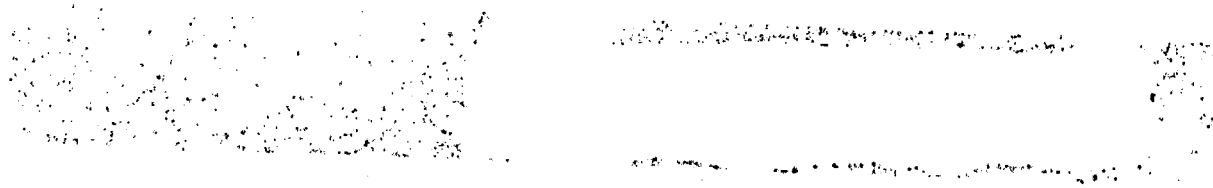

Printed in USA. Price $2.50. Available from the
Office of Technical Services
U. S. Department of Commerce
Washington 25, D. C.

LONGITUDINAL DISPERSION IN PACKED EXTRACTION COLUMNS

Contents

LONGITUDINAL DISPERSION IN PACKED EXTRACTION COLUMNS

Gabriel L. Jacques, John E. Cotter,
and Theodore Vermeulen
Lawrence Radiation Laboratory and Department of Chemical Engineering
University of California, Berkeley, California

April, 1959

ABSTRACT

Longitudinal dispersion (axial mixing) was studied for counter-current flow of liquids through packed beds, using six different combinations of packing type and size and bed arrangements. The Péclet Number, used as a dimensionless measure of the longitudinal dispersion coefficient, was measured in both the continuous and the discontinuous phase of the following systems: kerosene in water, water in kerosene, water in mineral oil. The observed values ranged from 100% to 10% of the Péclet number measured for the same packing in single-phase laminar flow.

Péclet numbers for each phase were correlated as a function of the two flow rates. An effect of packing diameter and sphericity on the continuous-phase Péclet number was also found. Different mechanisms were indicated for dispersion in the discontinuous phase, depending upon whether or not that phase wets the packing.

INTRODUCTION

Historical Survey

Packed columns are frequently selected as an effective and economical means of interphase contacting for liquid-liquid extraction. The usual method for designing an extractor involves computing the number of transfer units (NTU) required to bring about a given extraction, and multiplying by a height factor (the HTU) determined from previous experience on the subject.

The HTU concept, introduced by Colburn,[2,3] has been applied successfully to absorption towers; the application to extraction, however, has been less successful. HTU values vary widely with the types of system, the rates of flow, and concentrations, making it necessary to have at hand very specific data for the contemplated design.

Numerous experimental studies have been carried out, to measure the effective mass-transfer coefficients and HTU's in extraction columns, by such workers as Colburn and Welsh,[4] Laddha and Smith,[18] Koffolt, Row, and Withrow,[17] Sherwood, Evans, and Longcor,[24] Hou and Frankel,[10] Knight,[16] Elgin and Browning,[6] Johnson and Bliss,[14] and Allerton, Strom, and Treybal.[1] The data obtained have been reviewed by Elgin and Wynkoop[7] and by Treybal.[25] The HTU's for the individual phases are frequently correlated as some power of the flow-rate ratio, as by Rubin and Lehman,[23] but the result may be regarded as entirely empirical.

Over a twenty-year period it has remained impossible to interpret the experimentally measured performance of packed extraction columns in terms of mass-transfer theory and fluid and packing properties. The great difficulty encountered has suggested that the controlling variables are not solely those which determine the rate of mass transfer. Longitudinal dispersion is known to control the performance of multicomponent agitated reactors (from the work of Yagi and Miyauchi,[30] and of pulsed extraction columns (from studies by Vermeulen, Lane, Lehman, and Rubin[28]). Therefore, this investigation was undertaken to determine whether longitudinal dispersion could have a significant adverse effect upon the extraction performance of packed columns.

The physical picture of longitudinal dispersion is made up of two factors. The effect of backmixing, or local eddy motion, of packets of fluid may be characterized by a dispersion coefficient (E_i) which increases with increasing mixing. A velocity distribution, such as occurs with laminar flow in a pipe, will also appear as a dispersion effect. If there were no backmixing and the velocity profile were flat, a piston-flow model would be correct.

If longitudinal dispersion occurs in an extraction column, the concentration inside the inlet end of the column (for each phase) differs appreciably from that of the entering liquid, the driving potential for mass transfer is substantially reduced, and a longer column (for a given mass-transfer coefficient) is required to effect the same over-all separation.

Application of Continuity Equations

With knowledge of the dispersion coefficients (E_i) for the two phases, and of the mass-transfer coefficient, it is possible to write two simultaneous differential equations involving dispersion, following Miyauchi:[21]

$$d^2C_x/dZ^2 - P_xBdC_x/dZ - N_{ox}P_xB(C_x - mC_y) = 0, \qquad (1)$$

$$d^2C_y/dZ^2 + P_yBdC_y/dZ + N_{oy}P_yB(C_x - mC_y) = 0, \qquad (2)$$

with the boundary conditions

at $Z = 0$, $dC_x/dZ = P_xB(1-C_{xo})$ (3)

and $dC_y/dZ = 0$ (4)

at $Z = 1$, $dC_x/dZ = 0$ (5)

and $dC_y/dZ = P_yB(C_{y1} - C_y^1)$, (6)

where

P_i = Péclet number of the i phase (also denoted by N_{Pe}),

P_iB = $U_i\, h/E_i$ (also denoted by N),

B = h/d_p, where h is the column height and d_p is the particle diameter,

U_i = interstitial velocity of i phase,

Z = dimensionless length variable, ranging from zero at the x-feed end to unity at the feed end of the column,

C_i = dimensionless concentration in the i phase measured at a point Z; the number accompanying C, if a subscript, is the Z value inside the column; if a superscript (0 or 1), the Z value in the feed or product stream outside the column,

m = slope of equilibrium curve,

N_{oi} = true over-all number of transfer units for the i phase,

$N_{oy} = \Lambda N_{ox}$,

$\Lambda = \dfrac{m(U_o)_x}{(U_o)_y}$ = extraction factor,

$(U_o)_i$ = superficial velocity.

Equations (1) and (2) are differential equations of the second order, with constant coefficients. Their solution, obtained by differentiation and subsequent integration of a single fourth-order equation, gives the concentration at any point inside the column. Figure 1 shows the concentration profile in a typical extractor for piston flow (broken lines) and for Eqs. (1) and (2) (solid lines). The decreased driving force when backmixing occurs is shown graphically by the arrows. Miyauchi, McMullen, and Vermeulen[20] have provided graphical and tabular results corresponding to the solutions of Eqs. (1) and (2).

These workers have defined an apparent NTU, as given from Underwood's result[29], which is designated by a subscript P to indicate that it stems from a "piston-flow" model:

$$N_{oxP} = \frac{1}{1-\Lambda} \ln \left[\frac{1-\Lambda(1-X)}{X}\right], \qquad (7)$$

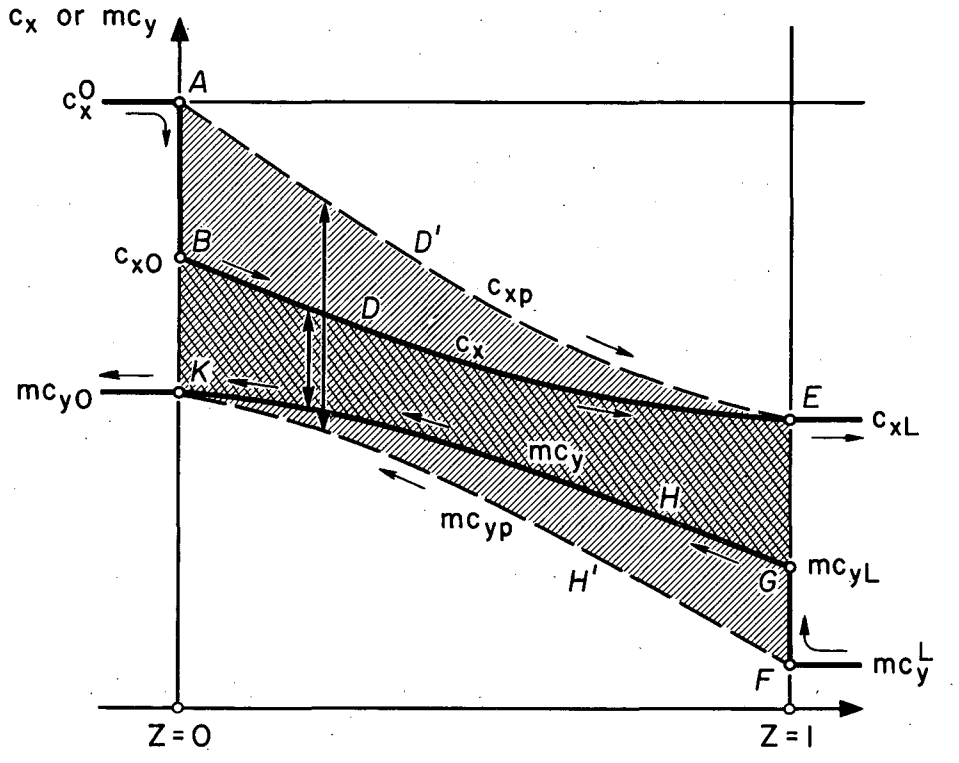

Fig. 1. Concentration profile in a typical extractor.

where

$$X = (C_{xl} - mC_y^l)/(1 - mC_y^l). \tag{8}$$

The true NTU can be related to the apparent NTU by a difference in reciprocals:

$$\frac{1}{N_{oxP}} - \frac{1}{N_{ox}} = \frac{1}{N_{oxD}} . \tag{9}$$

Here N_{oxD} is related to P_xB and P_yB by an approximate empirical equation

$$\frac{1}{N_{oxD} - \ell n\Lambda/(\Lambda-1)} = \frac{\Lambda}{f_x P_x B} + \frac{1}{f_y P_y B} , \tag{10}$$

where f_x and f_y are weighting factors which are functions of N_{ox} and Λ.[27] At $\Lambda = 1$, the term $(\ell n\Lambda)/(\Lambda-1)$ reduces to unity, and $f_x=f_y=1$.

By use of these relations, it should be possible to carry out any of the following calculations:

1. From an experimental C_{xl} and experimental P_xB and P_yB, to determine N_{ox}.

2. From an experimental C_{xl}, and a correlational N_{ox}, to determine an experimental N_{oxD} (by trial and error with N_{ox}).

3. From experimental or correlational P_xB, P_yB, and N_{ox} values, to predict the C_{xl} value for a column to be designed.

Statement of the Problem

The purpose of this report is to give experimental data and preliminary correlations of P_iB values for continuous, dispersed wetting, and dispersed nonwetting phases, in two-phase countercurrent flow through representative packings.

THEORETICAL ANALYSIS

Use of Breakthrough Curves

The column Péclet number values (P_iB) can be determined independently of any extraction operation, by tracer techniques for unsteady-state flow. Such methods involve the injection of a tracer into one phase, the tracer being insoluble in the other phase. The injection may have the mathematical form of a step function, a pulse function, or a sine-wave input; in this particular experimental program, a step function has been used. The resulting breakthrough curve is related to the dispersion coefficient E, and the derivation of equations for determining E from such a curve is outlined below.

Three alternate models are available for deriving the theoretical shape of the breakthrough curves: the diffusion model, unidirectional random walk, and multiple-stage perfect mixing. In the limiting case of a long bed, all models give essentially the same solution. For measurements on beds of different lengths under identical flow conditions, it is believed that the random-walk model gives more nearly identical values of Péclet number for short and long beds than either of the other models. Thus, even though the Péclet number is to be used in a diffusion-model equation for relatively long beds, it should be measured according to the random-walk model if the measurement is made in a short bed.

Diffusion Model

It is instructive to utilize the continuity equation for unsteady-state diffusion, even though the mechanism of dispersion does not coincide with that of eddy mixing in open-pipe flow. When this equation is written in terms of the dimensionless variable already defined, we have

$$\frac{\partial^2 C_i}{\partial Z^2} - P_iB \frac{\partial C_i}{\partial Z} - (P_iB)^2 \frac{\partial C_i}{\partial T} = 0. \qquad (11)$$

In order to use this solution it must be assumed that diffusion is continuous through the end of the actual column. Thus the equation can be solved for $Z \ll 1$, with NZ equal to the effective N value for the column length that is actually involved. Because of the unidirectional nature of the dispersion process, and because the same mathematical breakthrough curve is obtained with different N and Z values for the same value of NZ, Eq. (11) is believed to provide an accurate short-bed solution of the diffusion model. Since the equation has not been solved for a column in which breakthrough has penetrated to Z=1 --that is, for $\partial C_i/\partial T \neq 0$ -- use will be made of the boundary conditions for which a solution is already available:

$$Z = 0;\ C_i - 1 = \partial C/\partial T, \tag{12}$$

$$Z = 1;\ \partial C_i/\partial T = 0 \text{ and } C_i = 0. \tag{13}$$

Miyauchi[21] has obtained the solution

$$C_i = \sum_{n=0}^{n=\infty} \exp\left[\frac{NZ}{2}\left\{1 - \frac{T}{NZ}\left(1 + \left[\frac{2\mu_n}{N}\right]^2\right)\right\}\right] \times \tag{14}$$

$$\frac{N\mu_n[N \sin \mu_n Z + 2\mu_n \cos \mu_n Z]}{[(N/2)^2 + N + \mu_n^2][(N/2)^2 + \mu_n^2]},$$

where $N = P_i B$

and $$\mu_n = \cot^{-1}(\mu_n/N - N/4\mu_n).$$

Random-Walk Model

In flow through packed beds, individual elements of fluid do not all have the same velocity. If several elements enter the bed at the same time, their times of arrival at a plane downstream show a probability distribution. This velocity distribution results from laminar flow, from local eddying, and in some cases also from larger-scale channeling.

The unidirectional random-walk approach was first developed by Einstein[5] for the transport of sediment. Jacques[11] has extended this treatment to the case of fluid dispersion. This approach is believed to apply equally well to each liquid phase in a two-phase flow system.

The fluid phase involved, as a whole, may be considered to travel with characteristic velocity u, but in a series of discrete jumps corresponding to a mean free path L. If the total bed length is h, and the time that a particular portion of fluid has been in the bed is τ, then we can define a number of mixing lengths, N = h/L (corresponding to a column Péclet number), and a dimensionless time scale, T = uτ/L. When a material balance is applied to the final result, it develops that T = (Uτ/L)·(N + 1)/N, and hence that the characteristic velocity is related to the average linear velocity by the equation u = U·(N + 1)/N.

The eddy-dispersion coefficient E does not enter directly into the derivation, but its calculation is necessary in order to compare the results of the random-walk method with those of the diffusion theory. Thus, the eddy-dispersion coefficient can be defined as E = U·L, and it follows that N = hU/E. The particle Péclet number, N_{Pe}, is obtained upon multiplying N by the ratio d_p/h:

$$N_{Pe} = \frac{N \cdot d_p}{h} = \frac{d_p U}{E} \qquad (15)$$

The analysis is based upon the probability of finding any one packet of fluid at N mixing lengths and T time units after it has taken n jumps in its random walk. The probability is

$$p_T(N) = \sum_{n=0}^{n=\infty} [\exp(-N-T)] \frac{N^n}{n!} \frac{T^n}{n!} . \qquad (16)$$

This can be converted to a continuous function in normalized form,

$$p_T(N)dT = [\exp(-N-T)] I_o(2\sqrt{NT})dT. \qquad (17)$$

If a step-function concentration input is introduced at T=0 and N=0, such that $c_{(N=0)} = 0$ for T<0 and $c_{(N=0)} = c_o$ for T > 0,

$$x = \frac{c}{c_o} = \int_0^T \exp(-N-T)\, I_o(2\sqrt{NT})dT, \qquad (18)$$

with x increasing from zero toward unity as T increases toward infinity. It may be noted that x=1-J(T,N), using a function J derived to describe

heat and mass transfer in fixed beds.[26] A useful simplification for Eq.(18) as developed by Klinkenberg,[15] is

$$x = \frac{1}{2}\left[1 + \operatorname{erf}\left(\sqrt{T} - \sqrt{N} - \frac{1}{8\sqrt{N}} - \frac{1}{8\sqrt{T}}\right)\right]. \qquad (19)$$

The behavior of x as a function of T, at constant N, is shown in Fig. 2. The shape of the exponential breakthrough curve determines the applicable value of N, or column Péclet number, for the fluid phase involved.

Determination of N from Experimental Midpoint Slope

If Eq.(18) is differentiated with respect to T/N, at constant N we get

$$s = \partial x/\partial(T/N) = N(\partial x/\partial T), \qquad (20)$$

which can be written

$$s = \frac{N I_0(2\sqrt{NT})}{\exp(\sqrt{N}-\sqrt{T})^2 \exp(2\sqrt{NT})}. \qquad (21)$$

where s is the dimensionless slope.

If the slope s is to be evaluated at the midpoint of the curve, Eq. (18) or (19) must be solved to determine the T value at which x=0.5. This can be done most easily by calculating x at T=N, and using the average slope to find the increment of T that will bring x to a value of 0.5; the necessary steps are shown in Table I. It is seen that the increment is almost exactly constant, yielding the relation

$$(T)_{x=0.5} = N + 0.50, \qquad (22)$$

which can be used in subsequent calculations.

Table I. Calculation of T at x=0.5

N	$[50-100x_{(T=N)}]$%	Slope at x=0.5	Slope at T=N	Slope Average	$\frac{T}{N} - 1$	$(T)_{x=0.5}$
2	9.88	0.379	0.413	0.396	0.249	2.498
5	6.27	0.625	0.638	0.631	0.0944	5.497
10	4.45	0.892	0.899	0.896	0.0497	10.497
20	3.16	1.260	1.263	1.262	0.0250	20.501

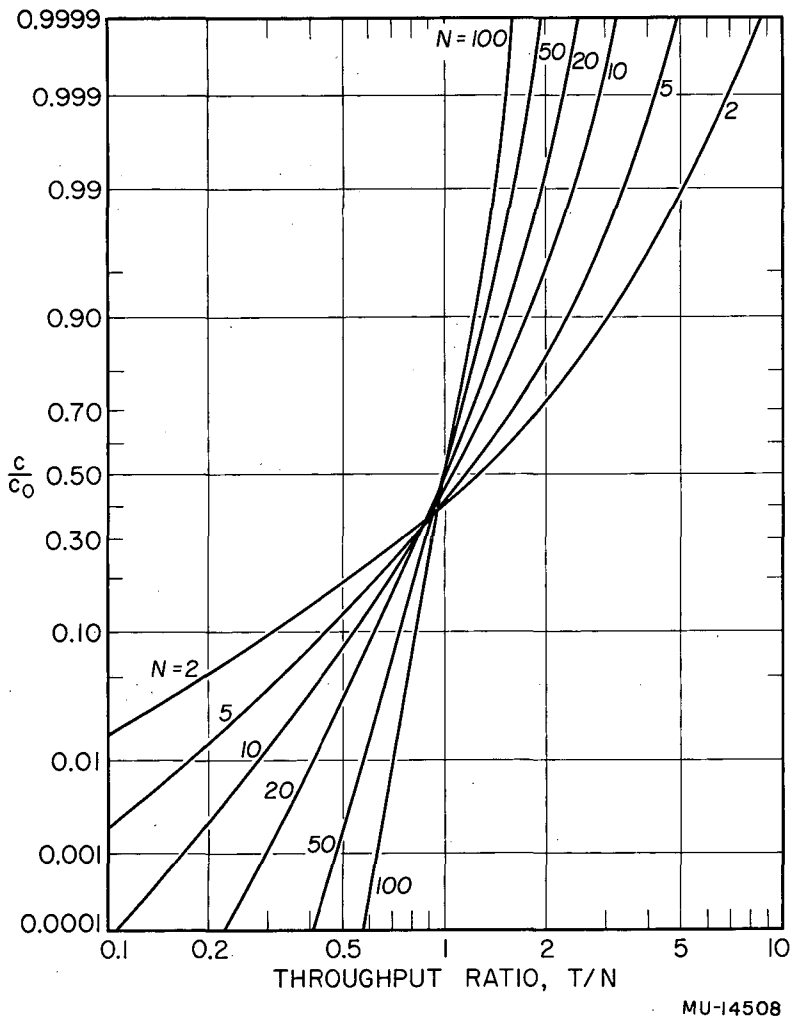

Fig. 2. Random walk breakthrough concentration.

The slope at this T can be calculated as the product of an asymptotic form and a quadratic correction term which is evaluated from the infinite-series expressions for the various terms in Eq. (21). For the I_o function, Jahnke and Emde[13] have given the series

$$I_o(2\sqrt{NT}) = \frac{e^{2\sqrt{NT}}}{2\pi(NT)^{1/4}} \left(1 + \frac{1}{16(NT)^{1/2}} + \frac{9}{512(NT)} + \ldots\right). \quad (23)$$

From well-known algebraic expansions, it can be shown also

$$[\exp(\sqrt{N} - \sqrt{T})^2]^{-1} = 1 + \frac{1}{16N} + \frac{17}{512N^2} + \ldots, \quad (24)$$

$$(NT)^{-1/4} = N^{-1/2}\left(1 - \frac{1}{8N} + \frac{1}{16N^2} + \ldots\right). \quad (25)$$

Substitution of these factors into Eq. (21) gives

$$s = \frac{\sqrt{N}}{2\sqrt{\pi}} \left(1 - \frac{1}{8N} + \frac{1}{8N^2} - \ldots\right). \quad (26)$$

However, in measuring the slope, one does not know the time corresponding to T=N. Therefore it is convenient to measure a slope s' with reference to a time scale of $\tau/\tau_{0.5}$ (with τ = time):

$$s' = dx/d(\tau/\tau_{0.5}) = \frac{T_{(x=0.50)}}{N} : s, \quad (27)$$

or

$$s' = \left(1 + \frac{1}{2N}\right) s = \frac{\sqrt{N}}{2\sqrt{\pi}} \left(1 + \frac{3}{8N} + \frac{1}{16N^2} + \ldots\right). \quad (28)$$

In using this equation to solve for N, it would be possible to plot N against s'. However, the accuracy in determining N can be improved by plotting the series-expansion term, or its square. A function β will be defined such that

$$N = 4\pi(s')^2\beta, \quad (29)$$

with

$$\beta = \left(1 + \frac{3}{8N} + \frac{1}{16N^2} + \ldots\right)^2 \quad (30)$$

Figure 3 is a plot of $(\beta-1)$ against $4\pi(s')^2$, which can be used in connection with Eq. (29). By use of the foregoing relations, a still simpler calculation method is found. We can write

$$N = 4\pi(s')^2 - \Delta$$
$$\approx 4\pi(s')^2 - 0.80. \qquad (31)$$

At $N=\pi$, $\Delta=0.895$; at $N=5$, $\Delta=0.805$; and in the upper limit, $\Delta=0.750$. A value of $\Delta=0.80$ will give an error of -0.1% at $N=5$, and a maximum error of 0.2% for $N>5$.

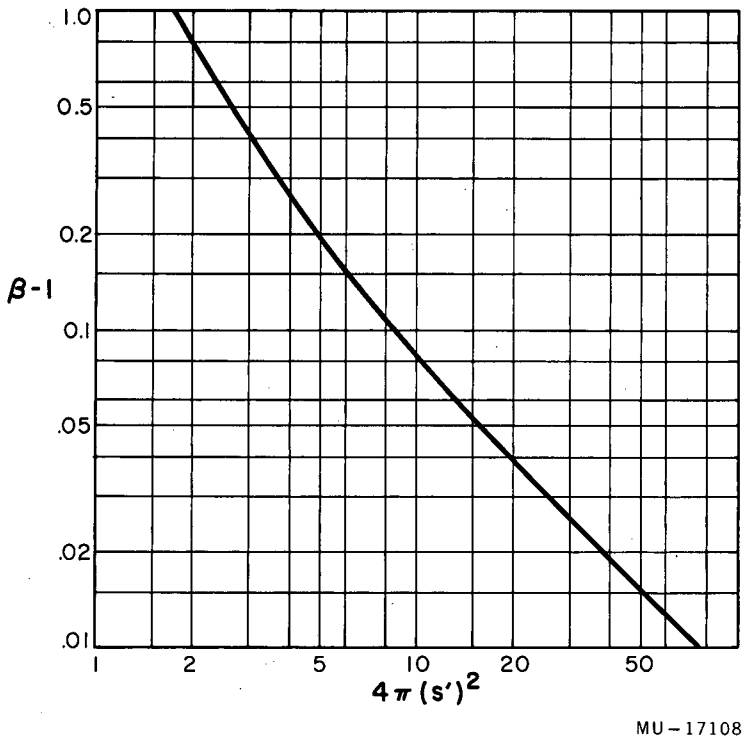

Fig. 3. Midpoint slope correction factor.

APPARATUS AND PROCEDURE

Apparatus

Columns

Six different columns were used for the investigation, three with ordered packings and octagonal or hexagonal cross sections, and three with random packings and circular or octagonal cross sections. The column dimensions are given in Table II and described in more detail by Jacques and Vermeulen.[12]

Column Heads

Expanded end sections, identical in construction, were connected above and below the particular packed section in use. As the columns were designed to operate in upward as well as in downward flow, the same accessories were adapted for both upper and lower end sections: two windows for visual observation and introduction of a photoelectric probe, a 6-inch-diameter inlet nozzle with interchangeable orifice plates designed to give a velocity profile as flat as possible, two symmetrically placed outlets, and a liquid-level control probe.

Conductivity Cells

Conductivity was used to determine the breakthrough curve for the aqueous phase. Conductivity cells were inserted in the packing, and also in the column head just below the interfacial level. These cells were of a special design to avoid disturbing the packing arrangement, and were constructed of two spherical sectors of 3/4-inch Bakelite balls connected by a pair of rhodium-plated pins. These cells were distributed among the sampling planes at 0, 3, 6, 12, 18, and 24 inches (nominal) for measurements on the continuous phase.

Photoelectric Probe

For use with a nonconducting discontinuous phase (kerosene), a photoelectric probe was also installed at the top of the column. A dye solution in kerosene (DuPont Oil Blue A) was introduced through the injection device, and the breakthrough curve was obtained and analyzed with a procedure similar to that used for conductivity measurements The probe

Table II

Dimensions and packings of experimental columns

Column number	Packing	Effective diameter (in.)	Arrangement	Distance between layers (in.)	Poro-sity (%)	Spher-icity	Height for continuous phase runs	Height for dispersed phase runs	Cross-sectional area ($in.^2$)
1	Spheres	0.75	Rhombohedral	0.53	26.0	1.0	23.6	24.4	30.3
2	Spheres	0.75	Orthorhombic-1	0.65	39.5	1.0	23.0	24.1	30.3
5	Spheres	0.75	Random	0.705	40.0	1.0	24.0	24.0	30.7
6	Spheres	0.75	Orthorhombic-2	0.75	39.5	1.0	24.0	25.2	30.6
10	Rings	0.50	Random	0.50	60.0	0.54	24.0	24.0	30.9
11	Spheres	0.38	Random	0.35	40.0	0.95	24.0	24.0	30.7

used was a modification of the apparatus developed by Langlois, Gullberg, and Vermeulen[19] in their determinations of interfacial areas. A photograph of the probe used is shown in Fig. (4). The upper (short) section holds the penlight bulb while the lower (long) section holds the RCA 1P41 (gas-filled) phototube. The gap between these two units could be varied as needed. Wiring diagrams for the lamp circuit and the photocell circuit are given by Jacques.[11]

Injection Tubes

The injection device was installed at the 0-inch nominal level, about 2 inches into the column. It consisted of several injection tubes connected to a manifold, the arrangement and number of tubes being dependent on the packing (seven tubes for hexagonal and random arrangements, and nine tubes for the octagonal columns). Each injection tube was made of annealed 302 stainless steel tubing (0.0625 inch o.d., 0.031 inch i.d.), and ran inside the packing through drilled aluminum balls, in order to minimize the disturbance of the arrangement.

Liquid-Level Control

The interface could be maintained at the top or bottom of the packing, depending on whether the water phase was continuous or dispersed. Two Teflon-covered nickel-rod probes were mounted in each head section for this purpose. These probes were slightly staggered in level to provide a neutral zone. Originally they were connected to a solenoid valve on the outlet water line, which was by-passed by a manually adjustable gate valve. Later a single-speed floating control was adapted, with all probes connected to a motorized-valve controller, and the column grounded to complete the circuit. With this system a probe would conduct when immersed in the water phase. The outlet water valve opened when both probes conducted and closed when neither did.

Piping Arrangement

The organic phase (kerosene or mineral oil) and tracer solution were piped from storage tanks with centrifugal pumps. Water was supplied from a constant-head tank, about 25 feet above the column, under gravity flow. The incoming flows were manifolded and valved, so as to meter each

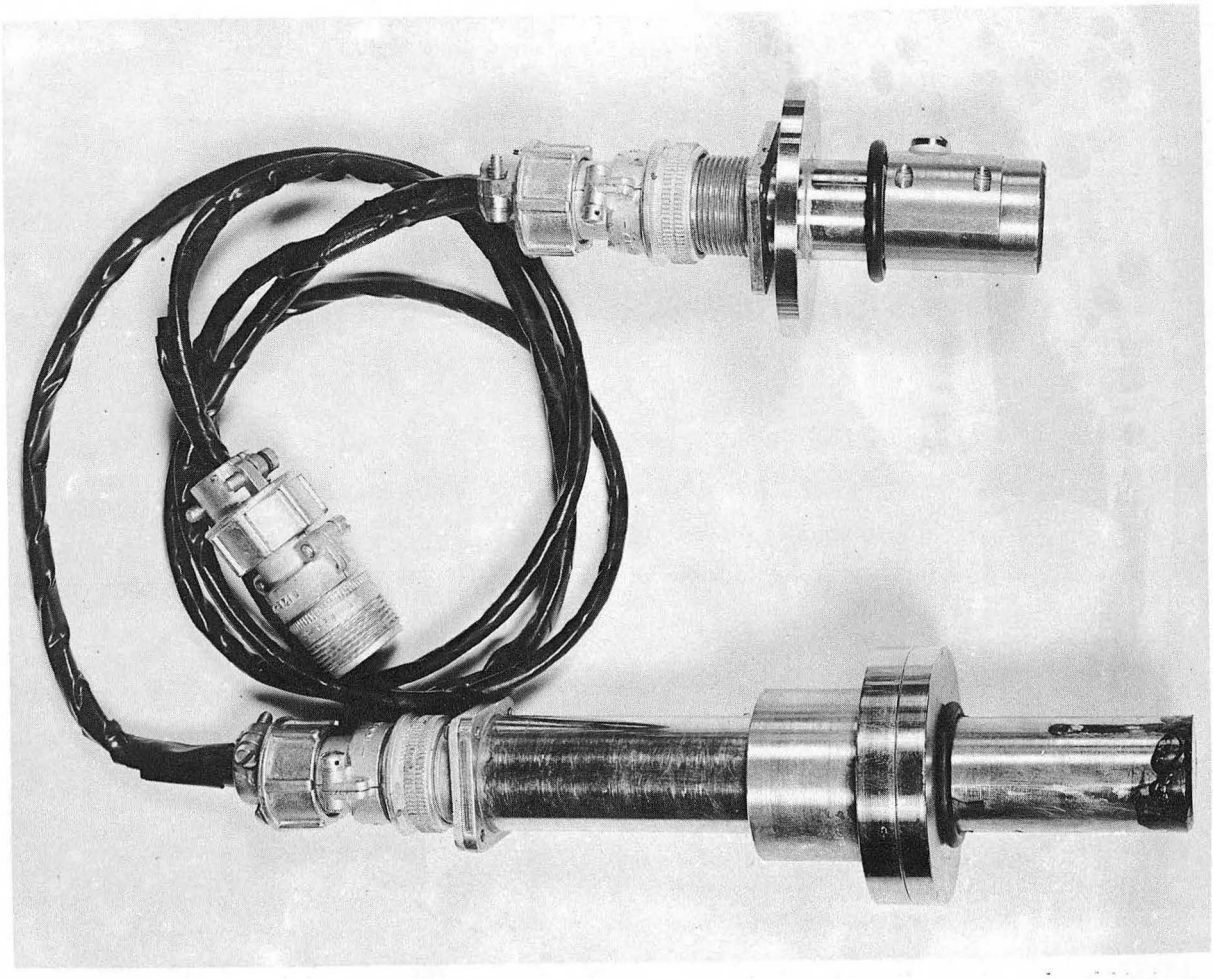

ZN-1815

Fig. 4. Interfacial area probe.

of them through the appropriate unit in a bank of six rotameters. The organic phase was returned to the supply tanks through an overhead line, and the water was dumped to the sewer.

Instrumentation

Changes in output concentration with time were measured by feeding a 1000-cycle constant current to the conductivity cell. The resistivity of the cell was measured by amplifying and rectifying the output signal, so as to monitor it continuously on a Leeds and Northrup Speedometer recorder.

The cell constants were determined by comparing the resistances measured in KCl or KNO_3 solutions of known concentration. The recorder readings were calibrated absolutely by use of a Helipot variable resistor.

Procedure

Start-Up

At the beginning of a run, the continuous phase was allowed to fill the column, and the dispersed phase was then introduced. Experimental measurements were made only at times when the interface was held within the neutral zone, following close adjustment of the outlet flow rates. This was essential for both continuous-phase and dispersed-phase measurements. First, if the outlet valve closes because of a level change, the continuous-phase flow rate in the column changes, affecting the dispersion rates in both phases. Second, for measurements of discontinuous-phase dispersion coefficients (which were made in a quiescent layer just below the coalesced interface), abrupt valve movement causes an irregular rate of flow at the point of measurement. Third, for a cell located close to the interface, the cell constant is strongly affected by the exact position of the interface.

Conductivity Measurements

When steady-state flows were reached, a small continuous injection of 1.0 N $NaNO_3$ solution was quickly begun. This time was noted by a pip on the strip-chart recorder. When the breakthrough curve leveled off to a steady-state value, injection was stopped. In some cases, a second strip-chart record was taken to measure the purging of the tracer

solution. The cell readings within the column fluctuated, owing to interference of droplets of the discontinuous phase in the conductance path. Also, the average cell-constant readings were higher than those for single-phase flow. For this reason in the continuous-phase runs (all using water as that phase) calibrations with tap water were made before and after each run, using the conductivity of the laboratory water supply, and maintaining the flow rates for both phases at constant values during both calibrations.

Resistance readings at uniform time intervals were read from the strip chart and were translated to conductivity values by use of the known cell constants. A relationship between concentration and conductivity of $NaNO_3$ solutions, as given by Jacques,[11] was used to convert the data to a plot of $(c-c_i)/(c_o - c_i)$ versus $\tau/\tau_{0.5}$, where c_i is the apparent $NaNO_3$ concentration corresponding to the conductivity of tap water The slope of this curve was then taken at $\tau/\tau_{0.5}=1$, and was used to calculate the column Péclet number by use of Eq. (31)

Photoelectric Measurements

The same steps as above were taken to set the liquid level and to establish steady-state flow in the column. A water-insoluble blue dye (dissolved in kerosene) was injected as a tracer. Measurements were also made by using uncolored kerosene, and taking the breakthrough curve for arrival of the discontinuous phase at the top of the column; good agreement was obtained between the two kinds of measurement, because there was almost no permanent holdup.

Either the color or the concentration of dispersed particles issuing from the packed section was followed with the photoelectric probe and millivolt recorder. The concentration-time curves were calculated from the voltage curves on the following basis. According to Langlois et al., the extinction ratio I_i/I (where I_i is the initial intensity and I is the transmitted intensity) can be expressed as

$$I_i/I = \omega A + 1 \qquad (32)$$

where A is the interfacial area of the discontinuous phase, and ω is a function of the ratio of the refractive indices of the phases. This

can be translated in terms of voltage readings from the recorder,

$$v/v_i = bA + 1 \tag{33}$$

where v and v_i are the voltage readings for the actual measurement and for the initial time, respectively. Finally, a plot of

$$\frac{v_f}{v}\ \frac{v - v_i}{v_f - v_i} = \frac{A - A_i}{A_f - A_i} \tag{34}$$

(where the subscript f indicates the final conditions at the end of the run) gives the breakthrough curve corresponding to the discontinuous phase.

For the transition from colorless to colored drops, extinction is due both to scattering and to molecular absorption of light. Since no theory is available for combining these two effects, and since very few runs of this type were made, the same calculation as above was also applied here.

Holdup

The holdup of dispersed aqueous phase was determined by allowing it to settle out of the column, then collecting it and measuring its volume. The column was first brought to a steady-flow condition, as before. With the interface at a known level, inlet and outlet flows were stopped. When the discontinuous-phase droplets had settled out of the packing, a secondary outlet was opened to a 5-inch i.d. decanter, and the collected aqueous phase was drained off to it until the level dropped back to its original position. The volume of liquid in the decanter represented the operational holdup. The column was then drained and flushed, all of the outlet going through the decanter. The final amount of collected liquid represented the total holdup, which was calculated as a percentage of the column void space.

Additional holdup data were calculated from the filling time for either the continuous or the discontinuous phase. This time could be obtained from the breakthrough plot, and corresponds to dimensionless time T=N+1. The holdup volume of the phase is given by the product of volumetric flow rate and filling time. Thus the foregoing procedures also provide a method of measuring the holdup.

Temperature for the Measurements

All runs were made at an ambient temperature of 68 ± 2°F. At this temperature, the kerosene used had a viscosity of 2.46 cp and a density of 0.820 g/ml., and the mineral oil had a viscosity of 22.0 cp and a density of 0.860 g/ml.

RESULTS AND DISCUSSION

Continuous Phase

Results

Measurements of longitudinal dispersion in the continuous phase, using the methods just described, are shown in Tables I-1 and I-2, in the Appendix, and summarized in Table III. Related data taken by Jacques are given in the Appendix, Tables II - 1 to II - 4.[11] These tables report both the packing Péclet number (N_{Pe_c}) itself, and its ratio to the single-phase Péclet number encountered for laminar flow (i.e., at comparable Reynolds numbers) in the same packing. The single-phase Péclet number in each case is the experimental value measured for single-phase flow, given in Fig. 5.

Table III. Summary of results - continuous phase

	F_c (gal/min)	F_d (gal/min)	$(N_{Pe})_c$	$(N_{Pe})_o$	$\frac{(N_{Pe})_c}{(N_{Pe})_o}$
A. Continuous Phase					
1. Kerosene in water, 0.50-inch Raschig rings	0.85	0.100	0.271	0.300	0.903
	0.351	0.100	0.137	0.300	0.457
	0.154	0.100	0.063	0.300	0.210
	0.578	0.100	0.204	0.300	0.680
2. Kerosene in water, 0.375-inch spheres	0.10	0.105	0.092	0.384	0.240
	0.05	0.100	0.040	0.384	0.104
	0.10	0.056	0.107	0.384	0.277
B. Single Phase					
1. Water, 0.375-inch spheres	0.30	0.0		0.384	1.0
2. Water, 0.50-inch Raschig rings	0.30	0.0		0.30	1.0

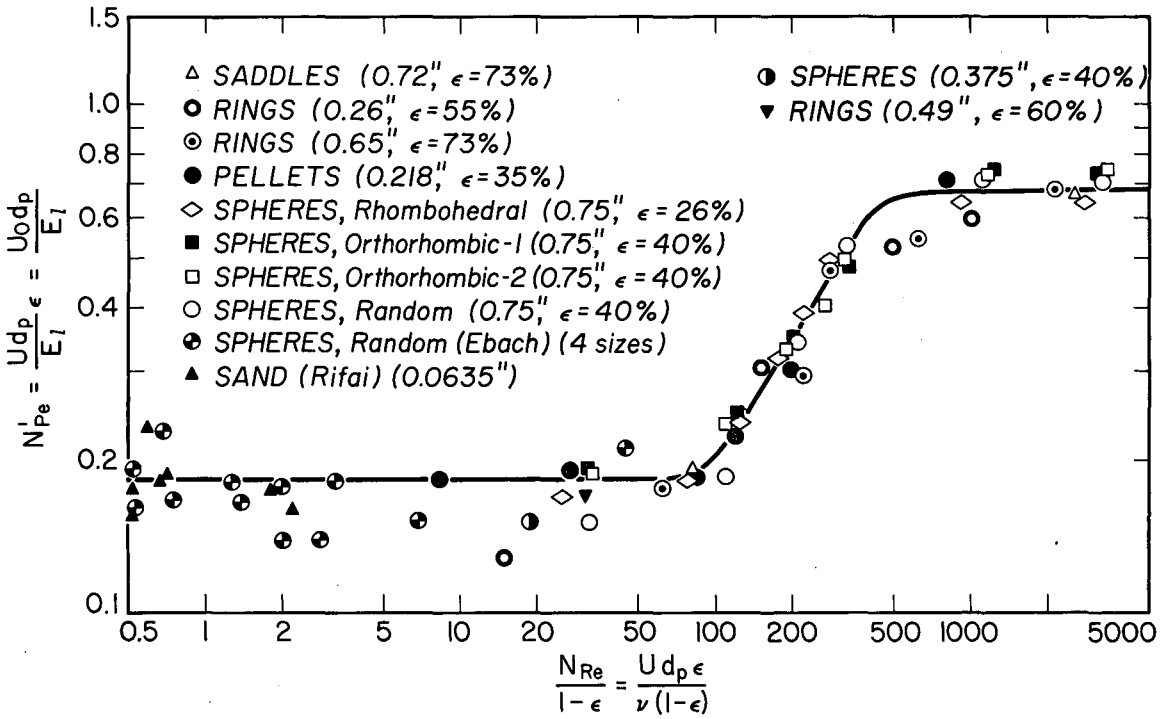

Fig. 5. Correlation for longitudinal dispersion in single-phase flow.

Péclet-number ratios for the continuous phase were found to be functions of the superficial velocity of the continuous phase, and also superficial velocity of the dispersed phase. One would expect Péclet numbers to be functions of the types of channels encountered by the flowing fluid. "Tortuosity" factors, empirical with the type of packing material, have been used by various workers to show the effect of the packing on the fluid flow.[8,22] Some measurable variables that affect the channel shapes are the size, sphericity, and porosity of the packing material. The present data have been correlated in terms of these variables, rather than tortuosity as such.

The resulting Péclet-number ratios for 0.75-inch stoneware spheres, taken by Jacques,[11] are shown in Figs. 6 and 7. Although $(N_{Pe})_o$ depends upon porosity, ϵ, the ratio $(N_{Pe})_c/(N_{Pe})_o$ does not; this is shown by nearly identical values of the Péclet ratio for 0.75-inch spheres, as functions of $(U_o)_d/(U_o)_c^2$, for both $\epsilon = 0.26$ and $\epsilon = 0.40$. An asymptote of 1.0 for the Péclet ratio indicates continuity between single- and two-phase flow, since $(N_{Pe})_c \rightarrow (N_{Pe})_o$ as $(U_o)_d \rightarrow 0$.

When particle diameter (d_p) and sphericity (ψ) are varied, as in the runs with 0.50-inch Raschig rings and 0.375-inch stoneware spheres, it develops that the group $d_p(U_o)_d/\psi(U_o)_c^2$ can be used as a dimensional correlating factor. The particle sphericity is defined as the ratio A_s/A_p, where A_s is the surface area of a sphere having the same particle volume, and A_p is the surface area of the particle. The continuous-phase ratio, $(N_{Pe})_c/(N_{Pe})_o$, is plotted against the correlating group mentioned above, in Fig. 8. The black (filled-in) points are for the kerosene-in-water system. Those for 0.50-inch Raschig rings and for 0.375-inch stoneware spheres have been obtained by Cotter, and establish the probable relative contributions of particle diameter and sphericity.

These results are compared with values calculated in this laboratory from breakthrough data given by Gomide;[9] the latter are shown as white (open) points, and were determined for the toluene-in-water system with 0.50-inch carbon Raschig rings and 0.375-inch stoneware rings and [illegible] saddles. The qualitative agreement obtained is believed to be within the accuracy of Gomide's single-run determinations, and this suggests that

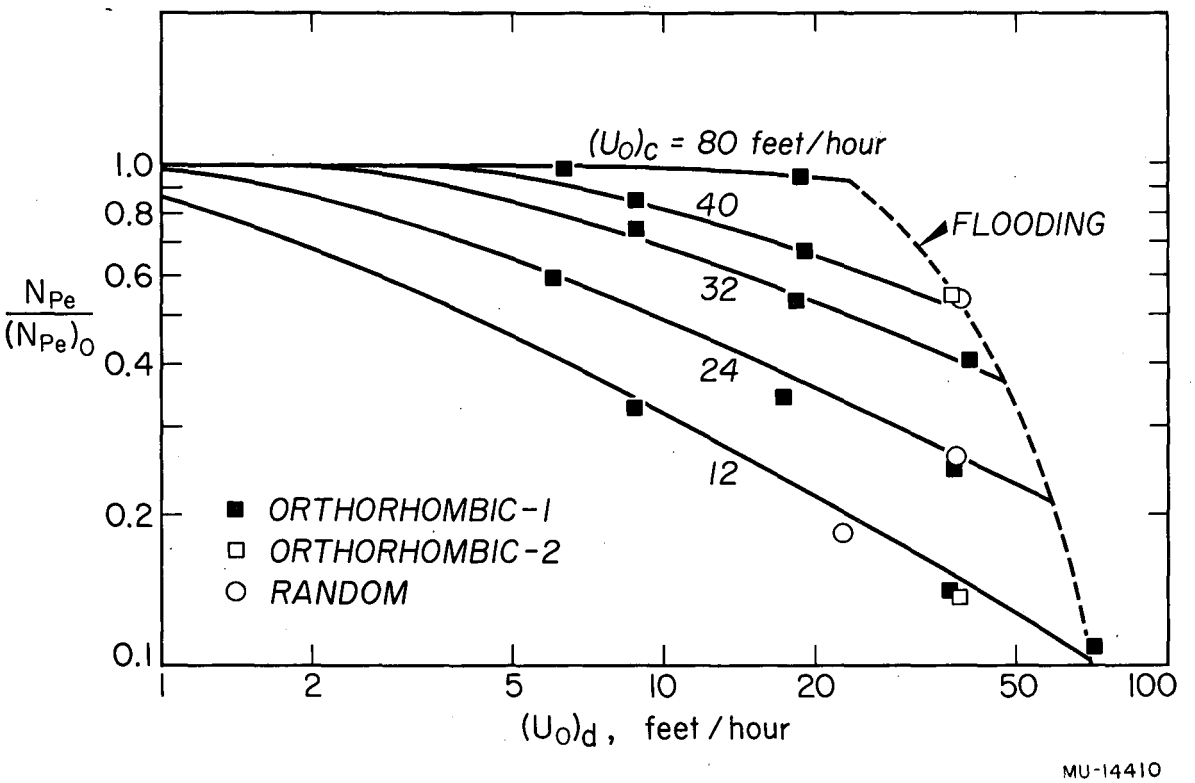

Fig. 6. Longitudinal dispersion in the continuous-phase for 0.75-inch sphere packing.

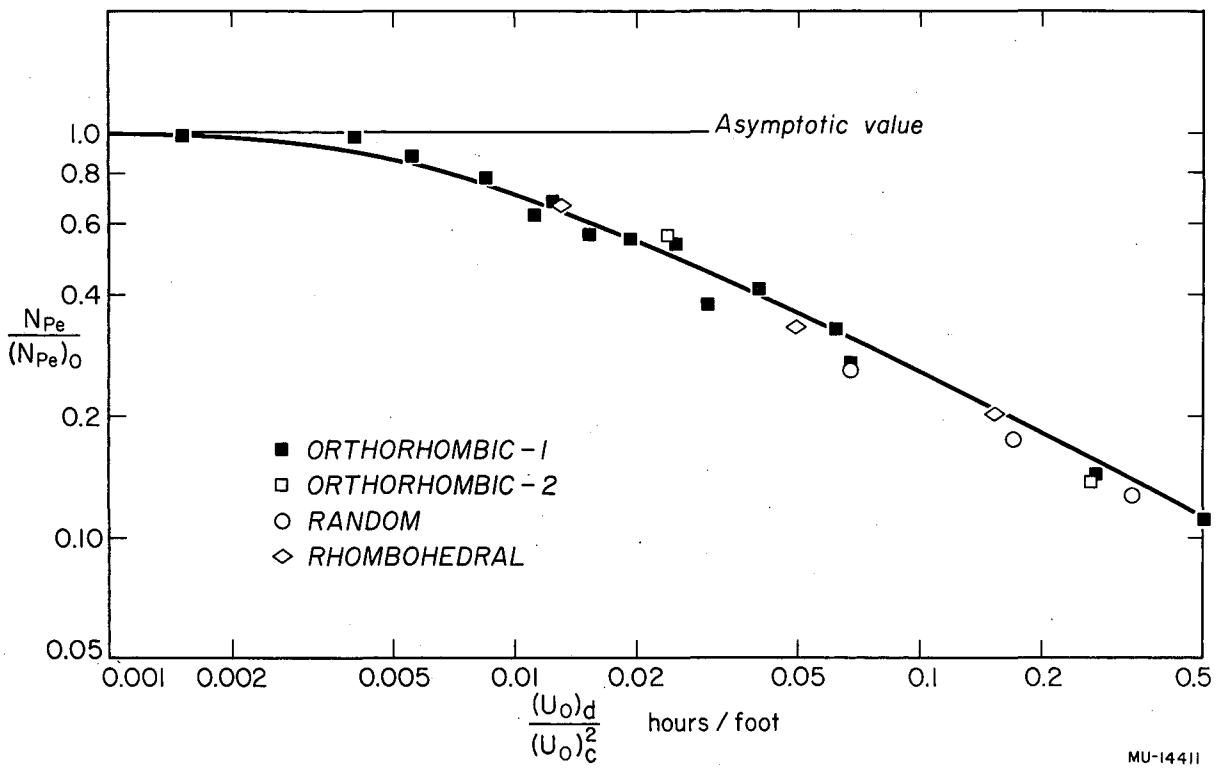

Fig. 7. Correlation for longitudinal dispersion in the continuous phase; kerosene dispersion in water, 0.75-inch spheres.

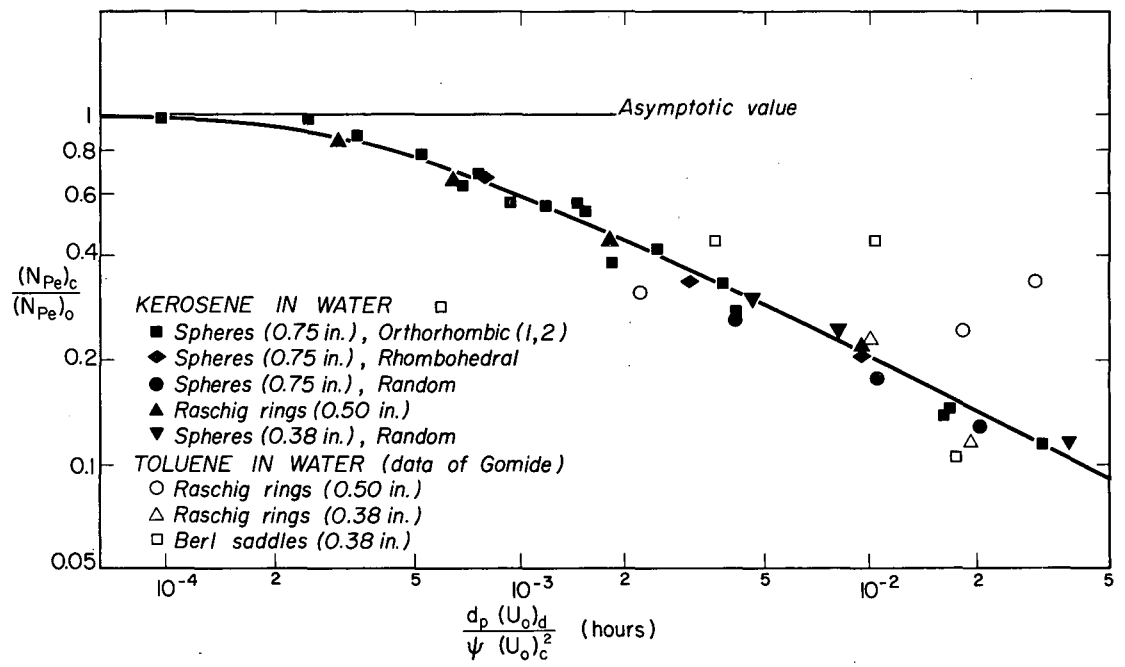

Fig. 8. Correlation for longitudinal dispersion in the continuous phase; collected data.

physical variables such as density differences and interfacial tension may have either negligible or compensating effects.

Discussion

In all cases the $(N_{Pe})_c$ values are less than $(N_{Pe})_o$, where $(N_{Pe})_o$ is independent of velocity. Since holdup of the dispersed phase reduces the pore space accessible to the continuous phase, it seems possible that holdup could be an important factor in determining the $(N_{Pe})_c$ behavior. However, $(N_{Pe})_c$ is observed to increase with increasing $(U_o)_c$ and to decrease with increasing $(U_o)_d$ (of Fig. 6), whereas increasing either velocity would increase the holdup (cf. Table I-8), and, through a porosity effect, increase $(N_{Pe})_c$.

An alternate mechanism for producing "back-mixing" in the continuous phase, compatible with the actual velocity effects, would be an entrainment (or intermittent backward flow) of the continuous phase caused by the motion of the dispersed-phase droplets. If this mechanism is correct, back-mixing should be greatest in the absence of internal circulation in the dispersed phase, in the presence of an intact outer surface for the droplets. Entrainment is clearly a factor that would increase (with reduction in $(N_{Pe})_c$) as $(U_o)_d$ is increased. The fact that an increase in $(N_{Pe})_c$ accompanies an increase in $(U_o)_c$ could correspond to a dilution of the entrainment, which would counteract its effect. This is the preferred model.

Dispersed Phase

Results

The results of dispersed-phase measurements are shown in Tables I-3, I-4, and I-5 in the Appendix. A summary of these results is given in Table IV. Jacques's data are in his Tables II - 5 and II - 6.[11] A Peclet-number ratio is again reported, this time as $(N_{Pe})_d/(N_{Pe})_o$.

Data from Jacques[11] for kerosene in water, using 0.75-inch stoneware spheres, are shown in Fig. 9. In this case the dispersed phase does not wet the packing. These data are included with a more extensive collection in Fig. 10, where $(N_{Pe})_d/(N_{Pe})_o$ is plotted against $(U_o)_c$. The black (filled-in) points give experimental results obtained in this

Table IV.

Summary of results - dispersed phase

		F_c (gal/min)	F_d (gal/min)	$(N_{Pe})_d$	$(N_{Pe})_o$	$\frac{(N_{Pe})_d}{(N_{Pe})_o}$
1.	Water in kerosene, 0.50-inch Raschig rings	0.034	0.086	0.095	0.300	0.317
		0.11	0.086	0.094	0.300	0.313
		0.364	0.086	0.074	0.300	0.247
		0.034	0.525	0.078	0.300	0.260
		0.364	0.31	0.07	0.300	0.233
		0.11	0.31	0.089	0.300	0.297
		0.74	0.525	0.086	0.300	0.287
		0.74	0.31	0.086	0.300	0.287
		0.74	0.086	0.086	0.300	0.287
		0	0.085	0.078	0.300	0.260
		0	0.31	0.086	0.300	0.287
2.	Water in mineral oil, 0.50-inch Raschig rings	0	0.083	0.103	0.300	0.343
		0	0.21	0.109	0.300	0.363
		0.15	0.083	0.120	0.300	0.400
3.	Water in kerosene, 0.75-inch spheres, orthorhombic-1	1.23	0.12	0.148	0.499	0.297
		1.23	0.32	0.10	0.499	0.200
		2.45	0.12	0.118	0.499	0.236
		2.45	0.32	0.046	0.499	0.092

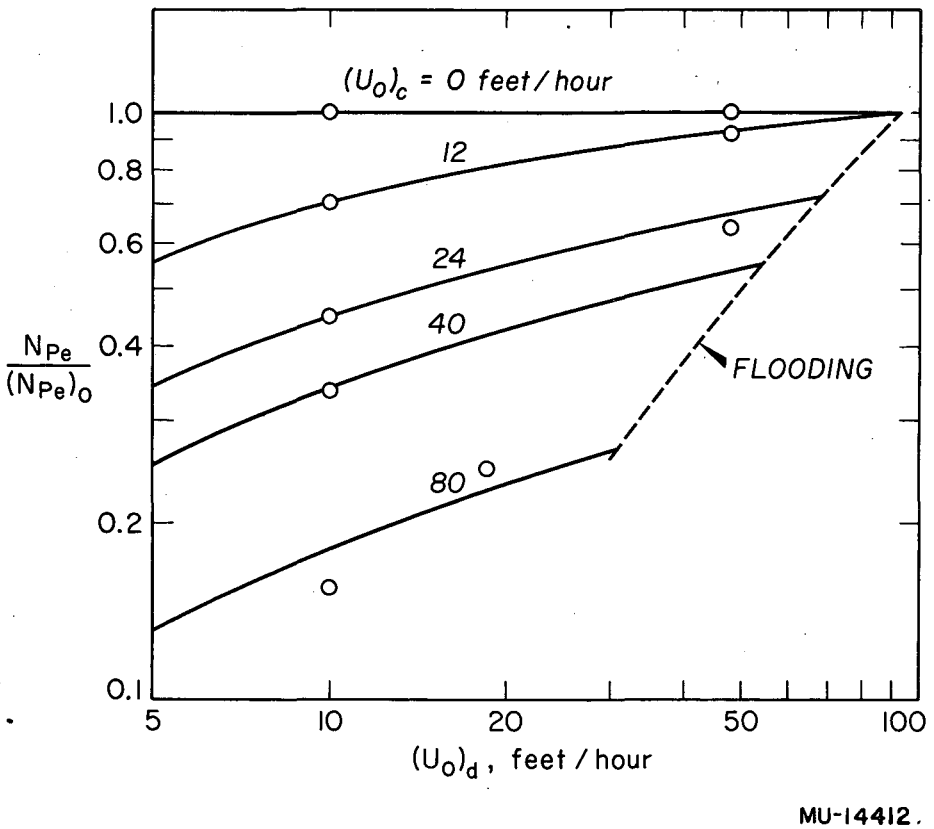

Fig. 9. Longitudinal dispersion in the discontinuous phase; kerosene dispersion in water, 0.75-inch spheres.

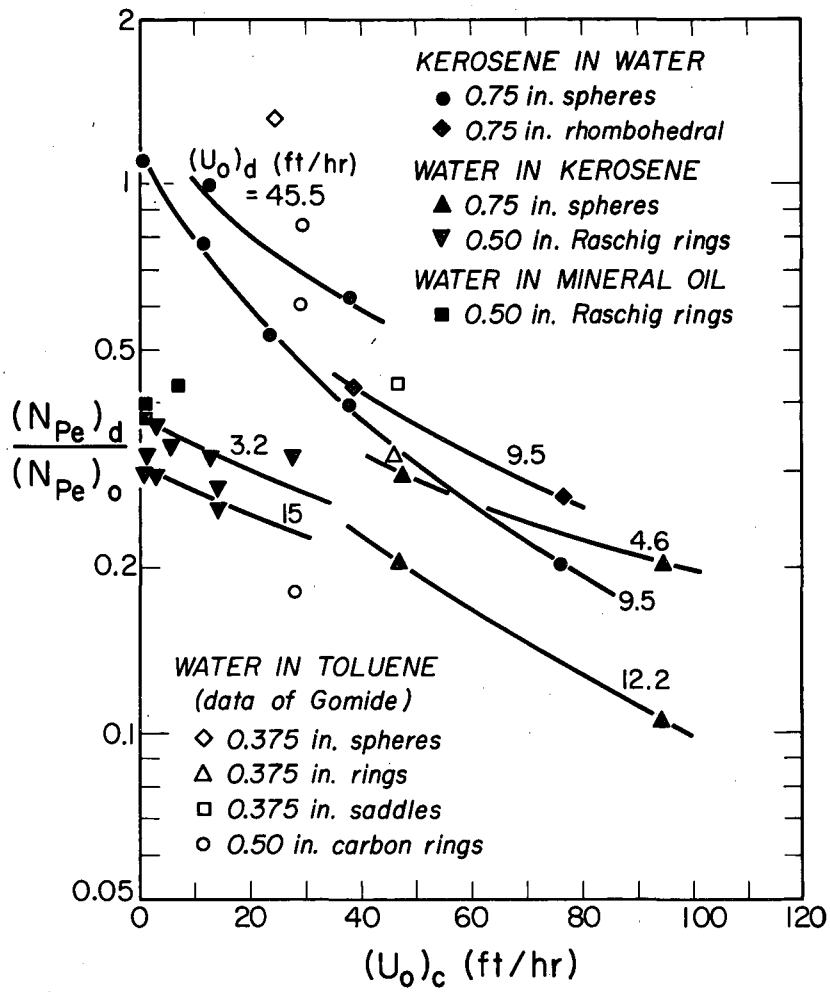

Fig. 10. Longitudinal dispersion in the discontinuous phase; collected data.

laboratory. Runs for water in kerosene, using 0.75-inch stoneware spheres and 0.50-inch stoneware Raschig rings, and for water in mineral oil, using 0.50-inch rings, were made by Cotter.

For comparison, Péclet ratios calculated from Gomide's results[9] are included as white (open) points; his data are for water in toluene, using 0.50-inch carbon Raschig rings and 0.375-inch stoneware Raschig rings, saddles, and spheres.

It may be seen from Fig. 10 that increasing $(U_o)_d$ has opposite effects on $(N_{Pe})_d/(N_{Pe})_o$, depending on whether the dispersion phase is a wetting or a nonwetting fluid with respect to the packing. It appears difficult to encompass the two widely differing types of observed behavior in a single general correlation.

In Fig. 11 the $(N_{Pe})_d/(N_{Pe})_o$ data of Jacques, for kerosene dispersed in water, are correlated as a function of the quotient $(U_o)_d/(U_o)_c^2$. Also shown are white (open) points from Gomide,[9] for water dispersed in toluene with 0.50-inch carbon Raschig rings.

Figure 12 shows $(N_{Pe})_d/(N_{Pe})_o$ data of Cotter, with water dispersed in stoneware packings, plotted as a function of the product $(U_o)_c\ (U_o)_d$. Data of Gomide, for wetting dispersed phase, are again indicated as white points.

Discussion

For a dispersed phase which preferentially wets the packing (water in kerosene), $(N_{Pe})_d$ decreases with increasing $(U_o)_c$ and $(U_o)_d$. This corresponds to an increased mixing length L, with a number of possible explanations. Since permanent holdup appears to increase with increasing $(U_o)_c$, and is perhaps accompanied by a decrease in the operating holdup, the effect of increasing $(U_o)_c$ may be to give a greater spread in velocity distribution in the dispersed phase.

An alternate explanation, leading to the same conclusion, is as follows: as $(U_o)_c$ increases, a wetting dispersed phase may tend to channel down the packing to a greater extent, thus traveling a greater average distance before recombination of streams, giving a longer effective mixing length.

With a nonwetting dispersed phase, $(N_{Pe})_d$ also decreases with

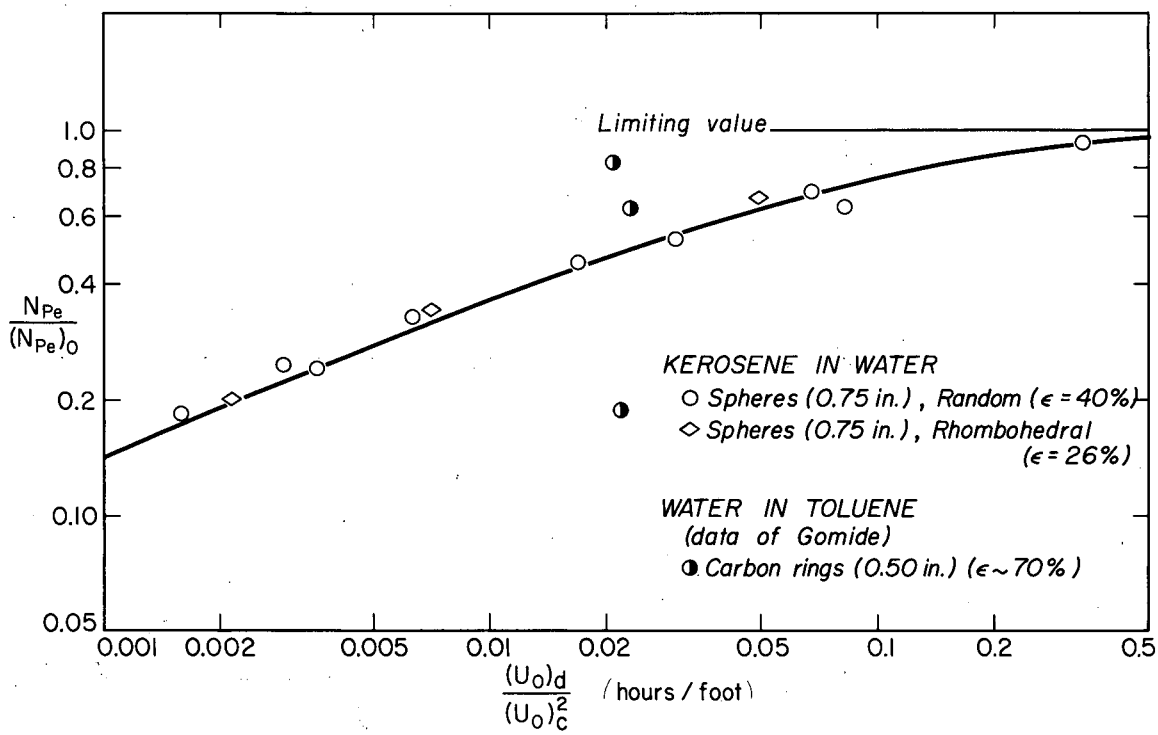

Fig. 11. Correlation for longitudinal dispersion in a non-wetting discontinuous phase.

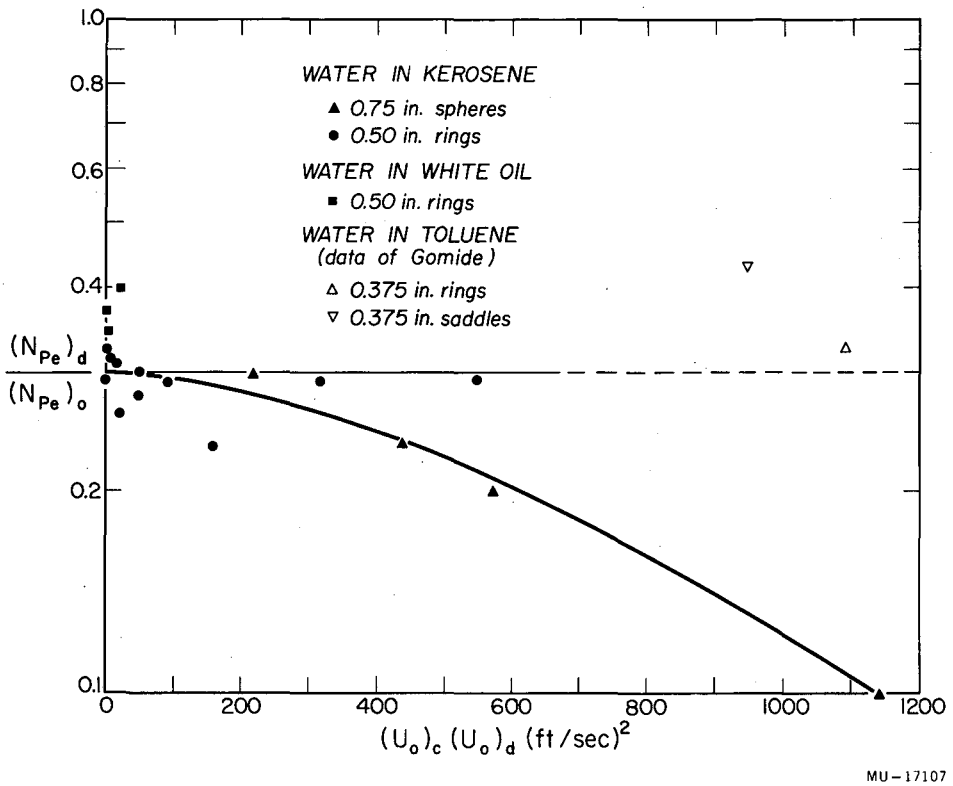

Fig. 12. Correlation for longitudinal dispersion in a wetting discontinuous phase.

increasing $(U_o)_c$. The argument for a more pronounced velocity distribution may still be valid. The effect of increasing $(U_o)_d$ is to increase $(N_{Pe})_d$. This explanation would require that increasing $(U_o)_d$ should reduce the velocity distribution (which is possible), and this increase gives a larger $(N_{Pe})_d$. The mechanism might be that a higher $(U_o)_d$ increases the probability of collisions between droplets and thus decreases the mixing length.

Holdup

Direct experimental measurements of holdup (χ_d) in the dispersed phase are given in Tables I-7 and I-8. They show that the holdup increases with both increasing continuous-phase and increasing dispersed-phase velocity. Furthermore, measurements with water dispersed in mineral oil suggest that permanent holdup is not a constant, but increases with increasing continuous-phase velocity. Measurements of indirect operational holdup, calculated from breakthrough curves for the continuous phase, are shown in Tables I-9 and I-10. Dispersed-phase total-holdup values are obtained by difference.

APPLICATION TO PACKED-COLUMN EXTRACTION

The experimental Peclet-number values obtained should be of direct use, in conjunction with experimental extraction data from an operating column, to determine the true mass-transfer rates in such a column. To illustrate the calculation, and also to determine the typical magnitude of the correction from apparent to actual rates, data from Colburn and Welsh[4] have been selected, in which the transfer resistances lie almost entirely in a single phase.

The method outlined previously (Eqs. (7)-(10)) does not give precise results when applied to this limiting case. However, since no appreciable change in concentration (or activity) occurs in the "inactive" phase -- which does not offer a transfer resistance (to water or to isobutanol) -- a separate algebraic result by Miyauchi[21] can be applied. Complete mixing of the inactive phase can be assumed, indicated by $P_y B = 0$. The applicable relation is then

$$N_{oxP} = \ell n \frac{N_{ox}(e^{-\lambda 2} - e^{-\lambda 1}) + \lambda_1 e^{-\lambda 2} - \lambda_2 e^{-\lambda 1}}{P_x B\,(1 + 4r)^{1/2}} ,$$

where

$$\lambda_1 = (P_x B/2)[1 + (1 + 4r)^{1/2}],$$

$$\lambda_2 = (P_x B/2)[1 - (1 + 4r)^{1/2}],$$

$$r = N_{ox}/P_x B .$$

A plot of this relation is given in Fig. 13.

Smoothed values for the apparent HTU were taken from Colburn and Welsh's work, at superficial velocity values (G_x) of 1000 lb/hr·ft^2 for the "active" phase. The steps involved in estimating the actual HTU values are given in Table V, and the resulting values are compared with the apparent HTU in Figs. 14 and 15 for the continuous and dispersed phases respectively. In this particular system, the ratio H_{xP} is seen to vary from 1.1 to 1.8 for the continuous phase, and from 1.6 to 1.85 for the dispersed phase.

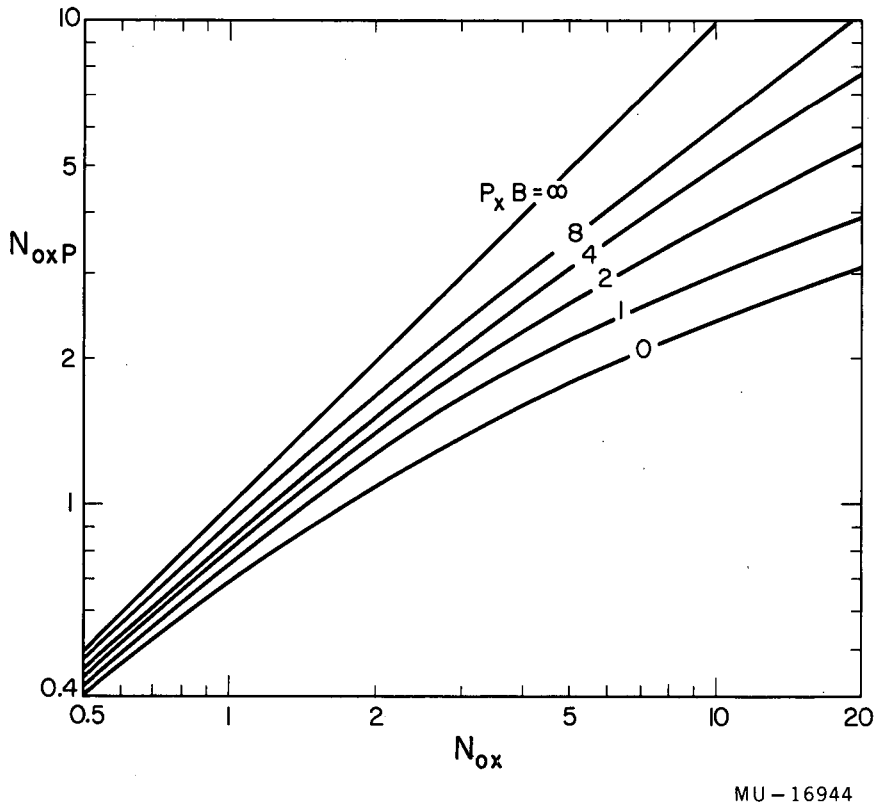

Fig. 13. $N_{ox}P$ as a function of N_{ox} and P_xB.

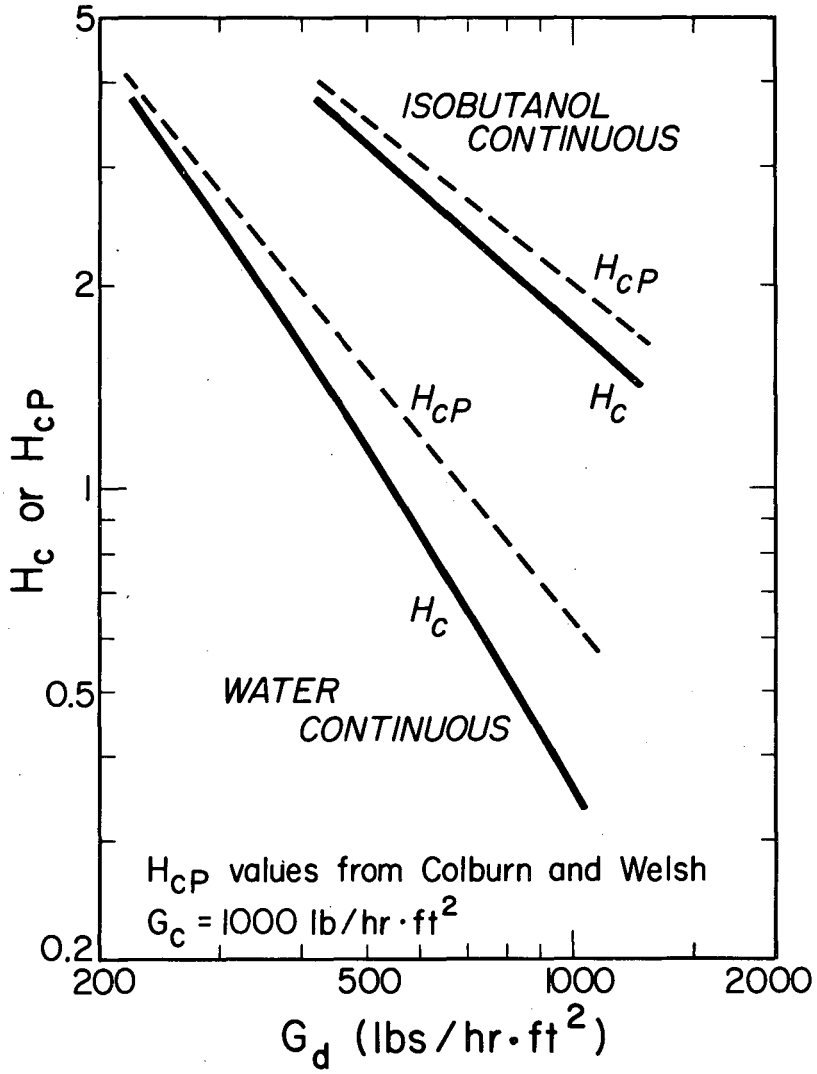

MU-17104

Fig. 14. H_c and H_cP for isobutanol-water system.

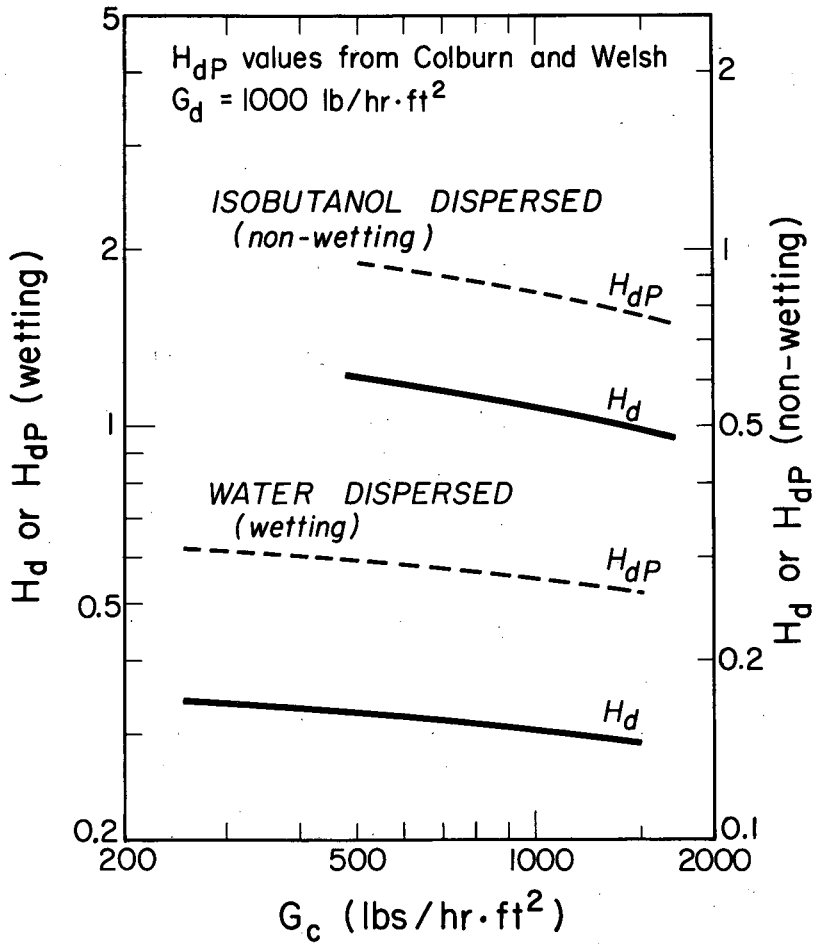

MU-17102

Fig. 15. H_d and H_dP for isobutanol-water system.

Table V.

Longitudinal Dispersion in Single-Phase Extraction Data

Water-Isobutanol Data of Colburn and Welsh[4]

(G_x = 1000 lb/hr·ft^2; Column height, 1.75 ft)

G_y	H_{xP}	N_{xP}	P_x/P_o	P_xB	N_x	N_{xP}/N	H_x
			CONTINUOUS PHASE: WATER				
250	3.500	0.500	0.480	6.000	0.540	0.926	3.241
500	1.500	1.170	0.330	4.150	1.450	0.807	1.211
750	0.870	2.010	0.280	3.530	2.900	0.693	0.603
1000	0.640	2.740	0.250	3.150	4.800	0.571	0.365
			CONTINUOUS PHASE: ISOBUTANOL				
500	3.500	0.500	0.470	5.910	0.540	0.926	3.241
750	2.600	0.680	0.390	4.910	0.770	0.883	2.300
1000	2.000	0.880	0.340	4.270	1.030	0.854	1.708
			DISPERSED PHASE: ISOBUTANOL				
500	0.930	1.880	0.170	2.140	3.000	0.627	0.583
1000	0.850	2.060	0.230	2.900	3.200	0.644	0.547
1500	0.750	2.340	0.270	3.400	3.650	0.641	0.481
			DISPERSED PHASE: WATER				
250	0.600	2.920	0.300	2.770	5.400	0.541	0.325
750	0.580	3.020	0.280	3.530	5.400	0.559	0.324
1250	0.520	3.360	0.270	3.400	6.230	0.539	0.280

* The phase under study is denoted as the X phase in each case

CONCLUSIONS

1. The continuous-phase axial Péclet number increases with increasing continuous-phase flow rate and decreases with increasing discontinuous-phase flow rate. This may be caused by intermittent entrainment of the continuous phase by the dispersed-phase droplets. The Péclet number ratio, $(N_{Pe})_c/(N_{Pe})_o$, is a function of $d_p(U_o)_d/(U_o)_c^2\psi$.

2. A nonwetting discontinuous-phase axial Péclet number decreases with increasing continuous-phase flow rate and with decreasing discontinuous-phase flow rate.

3. A wetting discontinuous-phase axial Péclet number decreases with both increasing continuous-phase flow rate and increasing discontinuous-phase flow rate.

4. Variation in the velocity distribution may be responsible for dispersed-phase Péclet behavior.

5. The Péclet number for a wetting discontinuous phase is usually lower than that for the continuous phase or for a nonwetting discontinuous phase. If backmixing in the discontinuous phase is the limiting factor in extraction-column performance, the fluid that wets the packing should generally be selected as the continuous phase.

ACKNOWLEDGMENT

Professors H. A. Einstein, J. M. Prausnitz, and D. R. Olander contributed substantially through helpful discussion. The authors also thank R. C. Gilmore and R. B. Waite for their part in construction of the experimental equipment, F. E. Vogelsberg for design and installation of electronic components, and Patricia Howard, Elizabeth Brecher, and Lilly Hirota for assistance in manuscript preparation. The work described was performed in the Lawrence Radiation Laboratory under the auspices of the U. S. Atmoic Energy Commission.

Table I-1

Continuous-phase Peclet numbers for kerosene in water; 0.50-inch Raschig rings; $(N_{Pe})_o = 0.300$

F_c (gal/min)	F_d (gal/min)	$(U_o)_c$ (ft/hr)	$(U_o)_d$ (ft/hr)	Run No.	s'	$(s')^2$	$(N_{Pe})_c$	$(N_{Pe})_c/(N_{Pe})_o$	$\frac{d_p(U_o)_d}{\psi (U_o)_c^2}$ - hr
0.85	0.10	31.8	3.74	68	1.000				
				69	1.150				
				70	1.000				
				Ave.	1.050 ±0.067	1.100	0.271	0.903 ±0.116	0.00031
0.351	0.10	13.1	3.74	71	0.750				
				72	0.750				
				73	0.800				
				Ave.	0.767 ±0.022	0.588	0.137	0.457 ±0.028	0.00180
0.154	0.010	5.76	3.74	74	0.450				
				75	0.550				
				76	0.665				
				Ave.	0.552 ±0.072	0.305	0.063	0.210 ±0.066	0.00940
0.578	0.10	21.6	3.74	77	0.950				
				78	0.900				
				79	0.900				
				80	0.920				
				Ave.	0.917 ±0.0175	0.841	0.204	0.680 ±0.027	0.00067

Table I-2

Continuous-phase Péclet numbers for kerosene dispersed in water; 0.375-inch spheres; $(N_{Pe})_o = 0.384$

F_c (gal/min)	F_d (gal/min)	$(U_o)_c$ (ft/hr)	$(U_o)_d$ (ft/hr)	Run No.	s'	$(s')^2$	$(N_{Pe})_c$	$(N_{Pe})_c/(N_{Pe})_o$	$\frac{d_p(U_o)_d}{\psi (U_o)_c^2}$
0.1	0.105	3.73	3.9	81	0.710				
				82	0.750				
				83	0.725				
				Ave.	0.728 ±0.0143	0.530	0.092	0.240 ±0.010	0.00820
0.05	0.10	1.86	3.73	84	0.535				
				85	0.500				
				Ave.	0.518 ±0.0175	0.268	0.040	0.104 ±0.009	0.03900
0.1	0.056	3.73	2.09	86	0.780				
				87	0.780				
				Ave.	0.780	0.608	0.107	0.277 ±0.000	0.00470

Table I-3

Dispersed-phase Peclet numbers for water dispersed in kerosene; 0.50-inch Raschig rings; $(N_{Pe})_o = 0.300$

F_c (gal/min)	F_d (gal/min)	$(U_o)_c$ (ft/hr)	$(U_o)_d$ (ft/hr)	Run No.	s'	$(s')^2$	$(N_{Pe})_d$	$(N_{Pe})_d/(N_{Pe})_o$
0.034	0.086	1.3	3.1	1	0.65			
				2	0.65			
				3	0.65			
				4	0.67			
				5	0.65			
				6	0.65			
				Ave.	0.653 ±0.0053	0.425	0.095	0.317 ±0.0057
0.11	0.086	4.14	3.2	7	0.70			
				8	0.70			
				9	0.65			
				10	0.67			
				11	0.60			
				12	0.60			
				13	0.65			
				14	0.65			
				15	0.63			
				Ave.	0.650 ±0.029	0.423	0.094	0.313 ±0.031
0.364	0.086	13.7	3.2	16	0.560			
				17	0.530			
				18	0.560			
				19	0.550			
				20	0.665			
				21	0.650			
				22	0.600			
				Ave.	0.588 ±0.043	0.346	0.074	0.247 ±0.042
0.034	0.525	1.3	19.6	23	0.600	0.360	0.078	0.260
0.364	0.31	13.6	11.6	24	0.550			
				25	0.600			
				Ave.	0.575 ±0.025	0.331	0.070	0.233 ±0.024
0.11	0.31	4.1	11.6	26	0.650			
				27	0.650			
				28	0.600			
				Ave.	0.633 ±0.022	0.401	0.089	0.297 ±0.023

Table I-3(cont'd.)

F_c (gal/min)	F_d (gal/min)	$(U_o)_c$ (ft/hr)	$(U_o)_d$ (ft/hr)	Run No.	s'	$(s')^2$	$(N_{Pe})_d$	$(N_{Pe})_d/(N_{Pe}$
0.74	0.525	27.7	19.6	29	0.650			
				30	0.600			
				Ave.	0.625 ±0.025	0.391	0.086	0.287 ±0.026
0.74	0.31	27.7	11.6	32	0.650			
				33	0.600			
				Ave.	0.625 ±0.025	0.391	0.086	0.287 ±0.026
0.74	0.086	27.7	3.2	33	0.600			
				34	0.625			
				35	0.650			
				36	0.630			
				Ave.	0.626 ±0.0138	0.392	0.086	0.287 ±0.014
0	0.085	0	3.2	37	0.600	0.360	0.078	0.260
0	0.31	0	11.6	38	0.625	0.391	0.086	0.287

Table I-4

Dispersed-phase Péclet numbers for water dispersed in mineral oil; 0.50-inch Raschig rings; $(N_{Pe})_o = 0.300$

F_c (gal/min)	F_d (gal/min)	$(U_o)_c$ (ft/hr)	$(U_o)_d$ (ft/hr)	Run No.	s'	$(s')^2$	$(N_{Pe})_d$	$(N_{Pe})_d/(N_{Pe})_o$
0	0.083	0	3.1	39	0.733			
				40	0.600			
				41	0.670			
				42	0.722			
				43	0.650			
				Ave.	0.675	0.456	0.103	0.343
					±0.042			±0.047
0	0.21	0	7.8	44	0.766			
				45	0.700			
				46	0.700			
				47	0.600			
				Ave.	0.692	0.479	0.109	0.363
					±0.0455			±0.052
0.15	0.083	5.6	3.1	48	0.667			
				49	0.733			
				50	0.767			
				Ave.	0.722	0.521	0.120	0.400
					±0.037			±0.044

Table I-5

Dispersed-phase Péclet numbers for water dispersed in kerosene; 0.75-inch spheres in orthorhombic-1 packing; $(N_{Pe})_o = 0.499$

F_c (gal/min)	F_d (gal/min)	$(U_o)_c$ (ft/hr)	$(U_o)_d$ (ft/hr)	Run No.	s'	$(s')^2$	$(N_{Pe})_d$	$(N_{Pe})_d/(N_{Pe}$
1.23	0.12	47	4.6	51	0.690			
				52	0.600			
				53	0.665			
				54	0.700			
				Ave.	0.664	0.441	0.148	0.297
					±0.0318			±0.033
1.23	0.32	47	12.2	55	0.500			
				56	0.600			
				57	0.575			
				58	0.585			
				Ave.	0.565	0.319	0.100	0.200
					±0.035			±0.031
2.45	0.12	93.5	4.6	59	0.570			
				60	0.625			
				61	0.625			
				62	0.600			
				Ave.	0.604	0.365	0.118	0.236
					±0.020			±0.019
2.45	0.32	93.5	12.2	63	0.400			
				64	0.455			
				65	0.500			
				66	0.385			
				67	0.365			
				Ave.	0.422	0.180	0.046	0.092
					±0.045			±0.030

Table E-6

Single-phase laminar flow; longitudinal dispersion

A. 0.375-inch spheres

F (gal/min)	U_o (ft/hr)	Run No.	S'	$(S')^2$	$(N_{Pe})_o$
0.30	12	88	1.420		
		89	1.420		
		Ave	1.420	2.020	0.384

B. 0.50-inch Raschig rings

F (gal/min)	U_o (ft/hr)	Run No.	S'	$(S')^2$	$(N_{Pe})_o$
0.30	12	90	1.100		
		91	1.100		
		Ave.	1.100	1.210	0.300

Table I-7

Discontinuous-phase holdup; water dispersed in mineral oil; 0.50-inch Raschig rings

F_c (gal/min)	F_d (gal/min)	χ_d, % void space				Ave χ_d %			Run No.
						oper.	perm.	total	
0	0.083	oper.	6.8	6.8	6.4 6.1	6.53	4.35	10.88	H1-H4
		perm.	4.4	-	- 4.3				
0	0.21	oper.	9.2	9.4	6.9	8.50	5.15	13.65	H5-H7
			-	4.4	5.9				
0	0.03	oper.	3.9	3.7	4.7	4.10	5.00	9.10	H8-H10
		perm.	5.1	5.7	4.3				
0.15	0.083	oper.	4.6	4.4	4.4 4.4	4.45	6.85	11.30	H11-H14
		perm.	-	-	6.5 7.2				

Table I-8

Discontinuous-phase holdup; water dispersed in kerosene; 0.75-inch spheres

F_c (gal/min)	F_d (gal/min)	χ_d % operational	Run No.
1.2	0.12	3.8	H15
1.2	0.32	7.0	H16
2.45	0.12	8.5	H17
2.45	0.12	12.2	H18

Table I-9

Continuous and discontinuous phase holdup
0.50-inch Raschig rings - Kerosene dispersed in water

F_c ft3/min	F_d gal/min	τ_{50} min	Run No.	$\frac{N+1}{N+0.5}$	$\chi_c\% = \frac{F_c \tau_{50} (100)(N+1)}{0.276\ (N+0.5)}$	$\chi_d\% = 100 - \chi_c$
0.114	0.100	2.07	68-70	1.037	88.65	11.35
0.047	0.100	5.7	71-73	1.070	93.33	6.67
0.021	0.100	10.8	74-76	1.138	93.25	6.75
0.075	0.100	3.1	77-80	1.048	93.50	6.50

Table I-10

Continuous and discontinuous phase holdup
0.375-inch spheres - Kerosene dispersed in water

F_c ft^3/min	F_d gal/min	τ_{50} min	Run No.	$\frac{N+1}{N+0.5}$	$\chi_c\% = \frac{F_c \tau_{50} (100)(N+1)}{0.184\ (N+0.5)}$	$\chi_d\% = 100 - \chi_c$
0.0134	0.105	12.0	81-83	1.077	94.23	5.77
0.0067	0.100	22.8	84-86	1.164	96.75	3.25
0.0134	0.056	12.1	86-87	1.059	93.10	6.90

Table II-1

Continuous-phase Péclet numbers with kerosene dispersed in water, 0.75-inch spheres, rhombohedral arrangement. $(N_{Pe})_Q = 0.661$.
(Data of G.L. Jacques)

Continuous flow rate, gal./min.	Discontinuous flow rate, gal./min.	Column height in.	Run No.	s'	$(N_{Pe})_c$	$(N_{Pe})_c/(N_{Pe})_Q$
0.30	0.158	23.6	702-2	0.84		
			702-3	0.84		
			703-5	0.80		
			703-6	0.88		
			703-9	0.85		
			Ave.	0.842	0.258	0.390 ± 0.0178
0.30	0.609	23.6	702-4	0.67		
			703-6	0.62		
			704-1	0.65		
			704-2	0.68		
			Ave.	0.655	0.146	0.221 ± 0.0152
0.60	0.158	23.6	628-9	1.09		
			629-10	1.10		
			630-1	1.12		
			630-3	1.10		
			630-4	1.13		
			Ave.	1.108	0.465	0.703 ± 0.0129

Table II-2

Continuous-phase Péclet numbers with kerosene dispersed in water, 0.75-inch spheres, orthorhombic-1 arrangement. $(N_{Pe})_{\infty} = 0.499$. (Data of G.L. Jacques)

Continuous flow rate, gal./min.	Discontinuous flow rate, gal./min.	Column height in.	Run No.	s'	$(N_{Pe})_c$	$(N_{Pe})_c/(N_{Pe})_{\infty}$
0.30	0.219	22.95	601-2	0.67		
			608-1	0.69		
			608-7	0.70		
			607-8	0.68		
			607-9	0.70		
			Ave.	0.688	0.168	0.337 ± 0.0143
0.30	0.951	22.95	529-4	0.50		
			530-3	0.47		
			604-4	0.50		
			609-5	0.48		
			Ave.	0.488	0.072	0.144 ± 0.0095
0.30	0.82	22.95	607-3	0.45		
			608-4	0.43		
			609-1	0.46		
			609-2	0.42		
			609-4	0.45		
			Ave.	0.442	0.054	0.108 ± 0.0105
0.60	0.158	22.95	602-7	0.92		
			603-1	0.88		
			605-2	0.90		
			605-3	0.87		
			605-7	0.95		
			605-9	0.90		
			Ave.	0.903	0.309	0.619 ± 0.0296
0.60	0.219	22.95	601-2	0.90		
			603-2	0.85		
			603-3	0.87		
			604-4	0.86		
			607-1	0.88		
			607-2	0.86		
			Ave.	0.87	0.284	0.569 ± 0.0177
0.60	0.426	22.95	521-1	0.72		
			521-2	0.69		
			521-3	0.67		
			602-4	0.70		
			602-5	0.73		
			602-10	0.74		
			Ave.	0.708	0.180	0.361 ± 0.0243

Table II-2 (cont'd.)

Continuous flow rate, gal./min.	Discontinuous flow rate, gal./min.	Column height in.	Run No.	s'	$(N_{Pe})_c$	$(N_{Pe})_c/(N_{Pe})_o$
0.60	0.951	22.95	529-1	0.62		
			602-6	0.64		
			604-3	0.62		
			621-5	0.65		
			621-7	0.635		
			Ave.	0.633	0.139	0.279 ± 0.0103
0.80	0.219	22.95	607-13	0.88		
			608-8	0.84		
			608-9	0.86		
			608-11	0.87		
			609-10	0.85		
			Ave.	0.860	0.278	0.557 ± 0.0160
0.80	1.00	22.95	607-6	0.75		
			607-13	0.78		
			609-11	0.73		
			610-1	0.79		
			610-2	0.72		
			Ave.	0.754	0.208	0.417 ± 0.0295
1.00	0.158	22.95	528-1	1.13		
			528-6	1.15		
			529-1	1.10		
			529-7	1.14		
			Ave.	1.130	0.498	0.998 ± 0.0265
1.00	0.219	22.95	523-3	1.07		
			525-1	1.05		
			525-2	1.06		
			527-5	1.03		
			527-6	1.05		
			528-2	1.02		
			Ave.	1.047	0.424	0.850 ± 0.0234
1.00	0.487	22.95	520-1	0.92		
			521-1	0.95		
			521-2	0.90		
			521-3	0.96		
			523-6	0.95		
			524-2	0.97		
			526-5	0.94		
			526-6	0.92		
			527-1	0.97		
			605-1	0.95		
			Ave.	0.939	0.336	0.673 ± 0.0285

Table II-2 (cont'd.)

Continuous flow rate gal./min.	Discontinuous flow rate gal./min.	Column height in.	Run No.	s'	$(N_{Pe})_c$	$(N_{Pe})_c/(N_{Pe})_\infty$
1.00	0.951	22.95	521-5	0.84		
			522-5	0.80		
			523-7	0.86		
			524-3	0.88		
			524-4	0.85		
			525-5	0.88		
			525-6	0.86		
			525-7	0.85		
			526-3	0.87		
			526-6	0.86		
			526-7	0.90		
			527-1	0.85		
			527-4	0.84		
			607-2	0.86		
			Ave.	0.857	0.275	0.551 ± 0.0256
2.00	0.23	22.95	606-4	1.04		
			606-7	1.12		
			606-8	1.15		
			606-9	1.10		
			Ave.	1.103	0.474	0.950 ± 0.0448
2.00	0.46	22.95	606-3	1.09		
			606-10	1.08		
			606-11	1.10		
			606-12	1.12		
			Ave.	1.100	0.471	0.944 ± 0.0215

Table II-3

Continuous-phase Péclet numbers with kerosene dispersed in water, 0.75-inch spheres, random arrangement. $(N_{Pe})_{\infty} = 0.358$. (Data of G.L.Jacques)

Continuous flow rate gal./min.	Discontinuous flow rate gal./min.	Column height, in.	Run No.	s'	$(N_{Pe})_c$	$(N_{Pe})_c/(N_{Pe})_{\infty}$
0.30	0.609	24.0	622-2	0.50		
			626-1	0.45		
			626-2	0.50		
			626-10	0.48		
			626-11	0.51		
			Ave.	0.488	0.068	0.191 ± 0.0185
0.30	1.21	24.0	622-5	0.42		
			624-1	0.45		
			625-1	0.43		
			Ave.	0.433	0.049	0.138 ± 0.0098
0.60	0.975	24.0	625-2	0.60		
			625-3	0.55		
			626-1	0.58		
			626-2	0.61		
			626-7	0.56		
			Ave.	0.580	0.107	0.301 ± 0.0239

Table II-4

Continuous-phase Péclet numbers with kerosene dispersed in water, 0.75-inch spheres, orthorhombic-2 arrangement. $(N_{Pe})_{\infty} = 0.476$. (Data of G.L. Jacques)

Continuous flow rate gal./min.	Discontinuous flow rate gal./min.	Column height, in.	Run No.	s'	$(N_{Pe})_c$	$(N_{Pe})_c/(N_{Pe})_{\infty}$
0.30	0.951	24.0	629-1	0.49		
			629-4	0.50		
			629-5	0.51		
			629-9	0.45		
			Ave.	0.488	0.068	0.143 ± 0.0141
1.00	0.951	24.0	627-1	0.88		
			627-2	0.89		
			627-4	0.90		
			628-2	0.86		
			628-5	0.87		
			Ave.	0.880	0.279	0.585 ± 0.0165

Table II-5

Discontinuous-phase Péclet numbers for kerosene dispersed in water, 0.75-inch spheres, rhombohedral arrangement. $(N_{Pe})_{\infty} = 0.661$. (Data of G.L. Jacques)

Continuous flow rate gal./min.	Discontinuous flow rate gal./min.	Column height, in.	Run No.	s'	$(N_{Pe})_d$	$(N_{Pe})_d/(N_{Pe})_{\infty}$
0.0	0.25	26.88	717-1	1.40		
			717-2	1.43		
			717-3	1.37		
			718-1	1.41		
			718-5	1.35		
			Ave.	1.390	0.654	0.989 ± 0.0453
0.0	0.60	25.88	718-4	1.16		
			718-6	1.18		
			720-3	1.20		
			Ave.	1.180	0.463	0.700 ± 0.0178
1.0	0.25	26.88	718-2	0.84		
			718-7	0.88		
			720-1	0.85		
			721-2	0.82		
			721-3	0.83		
			Ave.	0.844	0.227	0.343 ± 0.0165
2.0	0.25	26.88	721-5	0.67		
			722-1	0.70		
			722-3	0.67		
			Ave.	0.680	0.140	0.212 ± 0.0102

Table II-6

Discontinuous-phase Péclet numbers for kerosene dispersed in water 0.75-inch spheres, random arrangement. $(N_{Pe})_o = 0.356$. (Data of G.L. Jacques)

Continuous flow rate gal./min.	Discontinuous flow rate gal./min.	Column height, in.	Run No.	s'	$(N_{Pe})_d$	$(N_{Pe})_d/(N_{Pe})_o$
0.0	0.25	25.0	707-2	1.01		
			707-9	1.05		
			707-10**	1.03		
			707-11	1.07		
			Ave.	1.040	0.384	1.079 ± 0.0429
0.0	1.21	25.0	707-1**	1.05		
			707-8	1.07		
			Ave.	1.060	0.400	1.124 ± 0.0218
0.30	0.25	25.0	710-2**	0.88		
			710-3	0.90		
			710-7	0.84		
			711-5	0.92		
			Ave.	0.855	0.271	0.761 ± 0.0661
0.30	1.21	25.0	708-1	1.00		
			708-2	1.02		
			708-5	0.98		
			708-7	1.03		
			709-9	1.05		
			Ave.	1.016	0.365	1.025 ± 0.0436
0.60	0.25	25.0	713-2	0.72		
			713-4	0.74		
			713-5	0.75		
			Ave.	0.737	0.181	0.508 ± 0.0167
0.60	1.21	25.0	705-2**	0.86		
			705-3	0.84		
			705-10	0.87		
			706-9	0.88		
			Ave.	0.863	0.258	0.725 ± 0.0225
1.0	0.25	25.0	705-4	0.67		
			706-5	0.62		
			706-8**	0.64		
			706-9	0.65		
			Ave.	0.645	0.133	0.376 ± 0.0170

** In this and following tables, indicates runs using dyed kerosene.

Table II-6 (cont'd.)

Continuous flow rate gal./min.	Discontinuous flow rate gal./min.	Column height, in.	Run No.	s'	$(N_{Pe})_d$	$(N_{Pe})_d/(N_{Pe})_\infty$
1.0	1.21	25.0	705-5**	0.78		
			711-2	0.79		
			715-10	0.81		
			Ave.	0.793	0.213	0.598 ± 0.0180
2.0	0.25	25.0	705-1**	0.46		
			715-1	0.50		
			715-2	0.48		
			Ave.	0.480	0.063	0.177 ± 0.0129
2.0	0.46	25.0	712-1	0.61		
			712-3**	0.58		
			715-5	0.55		
			Ave.	0.580	0.103	0.289 ± 0.0239

Table II-7

Summary of Jacques's results
Continuous-phase Péclet numbers for kerosene dispersed in water
0.75-inch spheres

Arrangement	F_c gal/min	F_d gal/min	$(N_{Pe})_c$	$(N_{Pe})_c/(N_{Pe})_\infty$
Rhombohedral	0.30	0.158	0.258	0.390
	0.30	0.609	0.146	0.221
	0.60	0.158	0.465	0.703
Orthorhombic-1	0.30	0.219	0.168	0.337
	0.30	0.951	0.072	0.114
	0.30	1.82	0.054	0.108
	0.60	0.158	0.309	0.619
	0.60	0.219	0.284	0.569
	0.60	0.426	0.180	0.361
	0.60	0.951	0.139	0.279
	0.80	0.219	0.278	0.557
	0.80	1.00	0.208	0.417
	1.00	0.158	0.498	0.998
	1.00	0.219	0.424	0.850
	1.00	0.487	0.336	0.673
	1.00	0.951	0.275	0.551
	2.00	0.23	0.474	0.950
	2.00	0.46	0.471	0.944
Random	0.30	0.609	0.068	0.191
	0.30	1.21	0.049	0.138
	0.60	0.975	0.107	0.301
Orthorhombic-2	0.30	0.951	0.068	0.143
	1.00	0.951	0.279	0.585

Table II-8

Summary of Jacques's results, dispersed-phase Peclet numbers
Kerosene in water, 0.75-inch spheres

Arrangement	F_c gal/min	F_d gal/min	$(N_{Pe})_d$	$(N_{Pe})_d/(N_{Pe})_\omega$
Rhombohedral	0.0	0.25	0.654	0.989
	0.0	0.60	0.463	0.700
	1.0	0.25	0.227	0.343
	2.0	0.25	0.140	0.212
Random	0.0	0.25	0.384	1.079
	0.0	1.21	0.400	1.124
	0.30	0.25	0.271	0.761
	0.30	1.21	0.365	1.025
	0.60	0.25	0.181	0.508
	0.60	1.21	0.258	0.725
	1.0	0.25	0.133	0.376
	1.0	1.21	0.213	0.598
	2.0	0.25	0.063	0.177
	2.0	0.46	0.103	0.289

NOTATION

A	interfacial area
A_p	surface area of particle
A_s	surface area of sphere with volume of particle
B	h/d_p
C,x	dimensionless concentration
c	concentration
d_p	particle diameter
E	dispersion coefficient
F	flow rate
f	correlation weighting factor
h	height of column
H_{oi}	over-all height of transfer unit
I	transmitted intensity
I_o	zero-order Bessel function with imaginary argument
L	mixing length
m	slope of equilibrium curve
N_{oi}	number of over-all transfer units
N	Peclet number for the column
P_i, N_{Pe}	Peclet number for the packing
p	probability
s	midpoint slope of breakthrough curve
T	dimensionless time
U	mean interstitial velocity
u	characteristic velocity, in random-walk theory
U_o	superficial velocity
v	voltage
Z	dimensionless height
β	midpoint-slope correction factor
Δ	correction to approximate Peclet number
ϵ	porosity
Λ	extraction factor, $= m(U_o)_x/(U_o)_y$

τ	time
X	holdup, volume % of void space
ψ	sphericity
ω	light-transmission coefficient

Superscripts

0	feed end, outside column
1	solvent end, outside column

Subscripts

c	continuous phase
d	dispersed phase
D	dispersion, longitudinal
f	final
i	i phase
i	initial
n	number of jumps, in random-walk theory
o	final value (of concentration)
o	single phase (Peclet number)
P	apparent
x	x phase
y	y phase
0	feed end, inside column
1	solvent end, inside column
50	5.0% concentration point

Literature Cited

1. J. Allerton, B. O. Strom, and R. E. Treybal, Trans. Am. Inst. Chem. Engrs. 39, 361 (1943).

2. A. P. Colburn, Trans. Am. Inst. Chem. Engrs. 29, 174 (1939).

3. A. P. Colburn, Ind. Eng. Chem. 33, 459 (1941).

4. A. P. Colburn and D. G. Welsh, Trans. Am. Inst. Chem. Engrs. 38, 179 (1942).

5. H. A. Einstein, "Sediment Transport as a Probability Problem," Dissertation, Eidgenössische Technische Hochschule, Zurich, 1937.

6. J. C. Elgin and F. M. Browning, Trans. Am. Inst. Chem. Engrs. 31, 639 (1935).

7. J. C. Elgin and R. Wynkoop, in J. H. Perry, "Chemical Engineers' Handbook," 3rd ed.(McGraw-Hill Book Co., New York, 1950).

8. I. Fatt and H. Dykstra, Trans. Am. Inst. Mining, Met., Petrol. Engrs. 192, 249 (1951).

9. R. Gomide, "The Residence Time of Liquids in Extraction Packed Towers" (thesis), Massachusetts Institute of Technology, 1958.

10. H. L. Hou and N. W. Frankel, Chem. Eng. Progr. 45, 65 (1949).

11. G. L. Jacques, "Effect of Flow Conditions on Extraction Column Performance for Ordered and Random Packings" (thesis), UCRL-8092, November 1957.

12. G. L. Jacques and T. Vermeulen, A. I. Ch. E. Journal (paper submitted).

13. E. Jahnke and F. Emde, Funktiontafeln, 1st ed., Teubner, Leipzig, and Berlin, 100 (1909).

14. H. F. Johnson and H. Bliss, Trans. Am. Inst. Chem. Engrs. 42, 331 (1946).

15. A. Klinkenberg, Ind. Eng. Chem. 46, 2285 (1954).

16. O. S. Knight, Trans. Am. Inst. Chem. Engrs. 39, 439 (1943).

17. J. H. Koffolt, S. B. Row, and J. R. Withrow, Trans. Am. Inst. Chem. Engrs. 37, 559 (1941).

18. G. S. Laddha and J. M. Smith, Chem. Engr. Progr. 46, 195 (1950).

19. G. E. Langlois, J. E. Gullberg, and T. Vermeulen, Rev. Sci. Instr. 25, 360 (1954).

20. A. K. McMullen, T. Miyauchi, and T. Vermeulen, "Longitudinal Dispersion in Solvent Extraction Columns: Numerical Tables," UCRL-3911 - Suppl., January 1958.

21. T. Miyauchi, "Longitudinal Dispersion in Solvent Extraction Columns: Mathematical Theory," UCRL-3911, August 1957.

22. W. Rose, Trans. Am. Inst. Mining, Met., Petrol. Engrs. 186, 111 (1949).

23. B. Rubin and H. R. Lehman, Performance of Liquid-Liquid Extraction Equipment, UCRL-718, September 1950.

24. T. K. Sherwood, J. E. Evans, and J. V. A. Longcor, Trans. Am. Inst. Chem. Engrs. 35, 597 (1939).

25. R. E. Treybal, Liquid Extraction, (McGraw-Hill Book Co., New York, 1950).

26. T. Vermeulen, Advances in Chem. Eng. 2, 147 (1958).

27. T. Vermeulen, G. L. Jacques, J. E. Cotter, and T. Miyauchi, Am. Inst. Chem. Engrs. meeting, Atlantic City, March 1959.

28. T. Vermeulen, A. L. Lane, H. R. Lehman, and B. Rubin, A. I. Ch. E. Journal (paper submitted).

29. A. J. V. Underwood, Ind. Chemist 10, 129 (1934).

30. S. Yagi and T. Miyauchi, Kagaku Kikai (Chem. Eng., Japan) 17, 382 (1953); 19, 507 (1955).

Tables

Figures